J. Fluid Mech. (1991), *vol.* 227, *pp.* 309–343
Printed in Great Britain

The stability of countercurrent mixing layers in circular jets

By P. J. STRYKOWSKI AND D. L. NICCUM
Department of Mechanical Engineering, University of Minnesota, Minneapolis, MN 55455, USA

(Received 19 May 1990 and in revised form 26 October 1990)

A spatially developing countercurrent mixing layer was established experimentally by applying suction to the periphery of an axisymmetric jet. A laminar mixing region was studied in detail for a velocity ratio $R = \Delta U/2\bar{U}$ between 1 and 1.5, where ΔU describes the intensity of the shear across the layer and $\bar{U}$ is the average speed of the two streams. Above a critical velocity ratio $R_{cr} = 1.32$ the shear layer displays energetic oscillations at a discrete frequency which are the result of very organized axisymmetric vortex structures in the mixing layer. The spatial order of the primary vortices inhibits the pairing process and dramatically alters the spatial development of the shear layer downstream. Consequently, the turbulence level in the jet core is significantly reduced, as is the decay rate of the mean velocity on the jet centreline. The response of the shear layer to controlled external forcing indicates that the shear layer oscillations at supercritical velocity ratios are self-excited. The experimentally determined critical velocity ratio of 1.32, established for very thin axisymmetric shear layers, compares favourably with the theoretically predicted value of 1.315 for the transition from convective to absolute instability in plane mixing layers (Huerre & Monkewitz 1985).

1. Introduction

The dynamics of the axisymmetric jet have been studied for decades. Wille (1963), Bradshaw (1966), and Becker & Massaro (1968) described the initial development of a laminar jet as consisting of periodic vortex rings which were observed to coalesce and distort three-dimensionally as they travelled downstream. The spatial evolution of an axisymmetric mixing layer was examined in detail by Freymuth (1966) by applying monochromatic forcing to a circular jet. Freymuth compared his experimental results with the linear temporal and spatial theories developed by Michalke (1964, 1965) and demonstrated that the wave dispersion and the disturbance eigenfunctions could only be adequately described by adopting the spatial viewpoint. The measured spatial growth rates were lower than the theoretical predictions of Michalke (1965) for a hyperbolic tangent shear layer profile, but were in close agreement with the later calculations of Monkewitz & Huerre (1982) for a Blasius profile. Freymuth (1966) and Winant & Browand (1974) observed that the initial instability mode saturated and rolled up into organized structures constituting the so-called 'vortex rings'. Winant & Browand established further that the principal mechanism for the growth of the shear layer at low and moderate Reynolds numbers is by way of vortex amalgamation, a process which is controlled to a great extent by the randomness of the forcing applied to the mixing layer. When monochromatic forcing was used, the primary vortex structures became more regularly distributed in space, inhibiting their interaction, but if the mixing layer

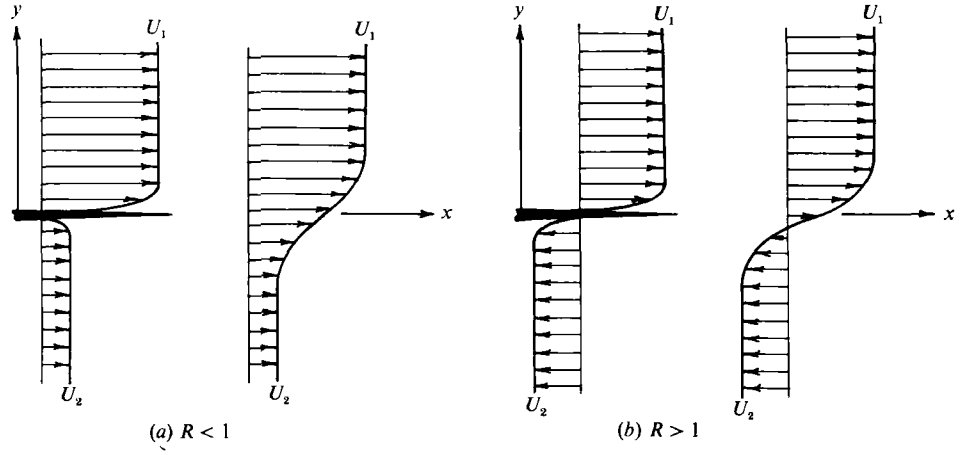

FIGURE 1. Spatially developing mixing layers defined by the velocity ratio $R = (U_1 - U_2)/(U_1 + U_2)$. (*a*) Coflowing mixing layer, and (*b*) counterflowing mixing layer.

was allowed to develop naturally, the random forcing of the background provided a 'jitter' to the vortex distribution, which facilitated the interaction. Petersen (1978), Drubka & Nagib (1981), and Ho & Huang (1982) examined the dispersive nature of the mixing region and indicated that the vortex pairing phenomenon is a consequence of a subharmonic resonance mechanism (Kelly 1967) between the primary vortex structures and a small-amplitude subharmonic wave.

The list of contributions given above is far from complete but serves to outline the richness of detail accompanying the transition in axisymmetric mixing layers. One common aspect of these studies is that the jet always exhausted into a quiescent environment. More precisely, the velocity ratio $R = \Delta U/2\bar{U}$ describing the jet mixing region is always equal to unity. The difference velocity $\Delta U = (U_1 - U_2)$ describes the intensity of the shear across the layer, where U_1 and U_2 are the uniform velocities on the high- and low-speed sides of the layer, respectively, and $\bar{U} = \frac{1}{2}(U_1 + U_2)$ is the average speed of the streams. In the most general case we can consider mixing-layer velocity ratios from zero to infinity, the former corresponding to a wake, and the latter to equal and opposite streams also known as the Kelvin–Helmholtz instability. When $R < 1$ a coflowing mixing region is established, as shown in figure 1 (*a*), where the streams U_1 and U_2 travel in the same direction. Coflowing mixing regions are typically generated downstream of a thin plate which provides an unambiguous frame of reference. Contributions to our current understanding of coflowing plane mixing regions are too numerous to mention here, but the works of Miksad (1972), Winant & Browand (1974), and Brown & Roshko (1974) serve as good examples; see Ho & Huerre (1984) for a complete reference list. Axisymmetric mixing layers having $R < 1$ – coflowing jets – were studied by Perry & Lim (1978) and Perry, Lim & Chong (1980).

When suction is applied to the underside of the splitter plate, as in figure 1 (*b*), a counterflowing mixing region is established where $R > 1$. To our knowledge a spatially developing counterflowing mixing region had not been systematically studied until quite recently by Strykowski & Niccum (1989), which is quite surprising given that countercurrent mixing in separated flows is so common. Humphrey & Li (1981) attempted to generate a spatially evolving mixing layer with $R > 1$ in a dual-contraction wind tunnel, but their novel approach proved to be

unsuccessful when a free-stagnation region was formed between the two streams. We must emphasize that the mixing regions depicted in figure 1 are allowed to develop spatially and are therefore not Galilean transformable. This is in contrast to countercurrent temporal mixing regions, which have been carefully examined by Thorpe (1968, 1971) and Ramshankar (1988).

The aim of the present study was to investigate a spatially developing mixing region having $R > 1$. We are motivated in part by the paucity of information available for velocity ratios greater than unity, but also by the expectation that dramatic changes might be observed in the neighbourhood of $R = 1.315$, where Huerre & Monkewitz (1985) predicted that the mixing layer would experience a transition from convective to absolute instability. An introduction to the linear stability theory of mixing layers will be given in §2 together with the related concepts of local and global instability. In §3 we will describe a method of generating a spatially developing countercurrent mixing region by applying suction to the periphery of a circular jet, and in §4 we will provide a description of the resulting mean velocity flow field. In §5 the spatial evolution of countercurrent mixing layers will be examined and compared with the spatial stability theory. The response of the jet column will be discussed in §6 together with a flow visualization study. We will inquire in §7 whether the phenomena we observe are the result of an unstable global mode. We will provide some concluding remarks in §8.

2. Spatio-temporal stability of the mixing layer

Huerre & Monkewitz (1985) employed a family of hyperbolic-tangent functions to model a plane mixing layer having velocity ratios greater than unity. Their analysis was novel because the stability of the mixing layer was treated from the combined spatio-temporal standpoint – accommodating a generic disturbance which could amplify simultaneously in space and time – in contrast to the earlier work of Michalke (1964, 1965, 1971) and Monkewitz & Huerre (1982) where either the temporal or spatial theory was investigated independently. (The spatial-temporal theory will be highlighted below, but the reader is referred to the work of Huerre & Monkewitz 1985 for a complete discussion.) The spatio-temporal theory is computed on an infinitely parallel base flow assuming small-amplitude disturbances (linear theory).

This initial value problem is solved by fixing the velocity ratio and establishing the response of the flow to an impulse-type vortical disturbance containing energy at all wavenumbers and frequencies. If the mixing layer is unstable, a disturbance will emerge from the initial impulse and amplify in both space and time over a finite range of frequencies and wavenumbers. When the group velocity of the unstable wave packet is positive everywhere, the disturbance will convect away from the source of the impulse and, after a sufficiently long time, leave the flow locally undisturbed. This constitutes *convective instability*. When the unstable disturbance contains the wavenumber having zero group velocity, then a wave will amplify in time but will remain stationary at the position where the impulse was introduced. Under these conditions the flow is *absolutely unstable*. Consequently, unstable vortical waves in convectively unstable flows will be detected by a fixed observer only if a constant excitation exists in the flow, such as the background turbulence level, surface roughness, or external excitation; similarly, the amplitude measured will depend on the level of the excitation.

On the other hand, during absolute instability some of the energy contained in the

impulse will never convect away but will amplify with time until a saturation amplitude is reached, no matter how small the amplitude of the initial impulse may have been. For this reason, absolutely unstable flows do not require a continuous disturbance source and are relatively insensitive to low-level external forcing. Furthermore, since all amplified disturbances convect away from the initial impulse, except the wave with zero group velocity, we can expect that the flow will be dominated by essentially a pure frequency instability (see discussion of Bechert 1985).

Huerre & Monkewitz (1985) identified a region of convective instability for hyperbolic-tangent mixing layers when $R < 1.315$ and a region of absolute instability when $R > 1.315$. The critical velocity ratio corresponds to $U_2/U_1 = -0.135$ indicating that relatively little reverse flow is necessary to establish absolute instability. In addition to the plane mixing layer, the spatio-temporal stability analysis was used to identify regions of absolute and convective instability in wakes (Koch 1985; Monkewitz & Nguyen 1987) and heated jets (Monkewitz & Sohn 1988). One of the major limitations of these analyses is that the flow is assumed to be locally parallel, which can be rigorously justified only if the disturbance wavelength is small compared to the streamwise variations of the flow field. This approach is called *local* analysis (see Huerre & Monkewitz 1990) and consists of computing the flow stability characteristics on a piecewise local basis, thereby mapping the flow stability in the streamwise direction. In the plane wake, for example, this approach identifies regions of *local absolute instability* in the near wake and regions of *local convective instability* farther downstream.

The overwhelming majority of laboratory flows are spatially evolving and only nominally two-dimensional. Chomaz, Huerre & Redekopp (1988) and Monkewitz (1988) examined the utility of local analysis in predicting the response of non-parallel flows and concluded that a finite region of the flow must be locally absolutely unstable, if a *global* mode is to emerge and the flow is to become *self-excited*. An unstable global mode is the result of the temporal amplification of a small-amplitude vortical disturbance everywhere in the flow domain giving rise to self-sustained oscillations in the absence of external forcing; the global mode is a solution of the linear-stability problem based on a two-dimensional, non-parallel base flow. Some advances have been made in identifying unstable global modes through stability calculations (Jackson 1987; Zebib 1987) as well as numerical studies (Hannemann & Oertel 1989; Karniadakis & Triantafyllou 1989). However, these computations have been limited to two-dimensional wakes.

Much of our current understanding of global instability was obtained by way of laboratory experiment. Huerre & Monkewitz (1990) describe these experiments as providing either direct or circumstantial evidence that an unstable global mode emerges depending on whether transient or stationary analysis is undertaken. Within these two broad classes of experiments, unstable global modes were identified in wakes (Mathis, Provansal & Boyer 1984; Provansal, Mathis & Boyer 1987; Sreenivasan, Strykowski & Olinger 1987) and heated and low-density jets (Sreenivasan, Raghu & Kyle 1989; Kyle & Sreenivasan 1989, and Monkewitz *et al.* 1990).

One of the goals of the present study is to determine if global instability could be established in the counterflowing jet by creating local absolute instability in the jet shear layers ($R > 1.315$). The results reported below show that highly energetic oscillations exist in the jet shear layers when the velocity ratio is elevated above $R = 1.32$, and that these oscillations produce long-lasting effects in the development

of the jet core downstream. We believe the results provide further insight into the relationship between local/global instability in spatially developing flows and, in particular, the extent to which local flow modifications can be used to produce global flow changes.

3. Experimental facilities and instrumentation

3.1. *Counterflowing jet facility*

A spatially developing, countercurrent mixing region can be generated by applying suction to the periphery of a circular jet. The counterflowing jet nozzle is shown in figure 2. The forward velocity stream U_1 is generated by passing air from left to right through the central nozzle, where it exits into a quiescent laboratory. The reverse velocity stream U_2 is produced by applying suction to a cavity which surrounds the inner nozzle. An unambiguous reference frame is provided by the splitter plate dividing the forward and reverse streams; the axial coordinate x is measured from the nozzle lip and is positive in the direction of the forward stream U_1. The inner nozzle was carefully machined on a CNC lathe from alloyed aluminium using a fifth-order polynomial contour requiring that both the slope and curvature vanish at the nozzle inlet and outlet. Special care was taken to ensure the integrity and concentricity of the inner- and outer-nozzle surfaces at the exit, where they form a fine knife edge. The inner nozzle has an area ratio of 25:1 and exits with a diameter of 2.54 cm. The outer nozzle was machined on the CNC lathe from rigid grey PVC and provides an exit slot width of 1.27 cm. A manifold consisting of 16 equally spaced ports was used to draw air through the outer nozzle and generate the reverse stream U_2.

The wind tunnel arrangement sketched in figure 3 supplies a high-quality air stream to the inner nozzle. The tunnel is driven by a Paxton Rm-80 centrifugal blower and a Toshiba speed controller; the blower vibrations were effectively isolated from the tunnel and room floor by a flexible coupling and rubber-in-shear mounts. The air exiting the blower is passed through a diffuser section followed downstream by a large-aspect-ratio honeycomb and screen before exhausting into a 28-cm-diameter plenum chamber. The plenum chamber is followed by a carefully machined fifth-order polynomial nozzle having an exit diameter of 12.7 cm. The air is passed through a second smaller plenum chamber and several screen combinations before encountering the final contraction; the total system length is approximately 6 m. Circumferentially placed holes were machined into the section upstream of the diffuser and act effectively as a Helmholtz resonator reducing the acoustic waves found in the tunnel; a twofold reduction in the exit turbulence intensity is possible using this arrangement. The combination of flow manipulators consistently provided a turbulence intensity of 0.1 % for all measurements presented here. The turbulence intensity is based on long-time averages (typically 20 s) of the streamwise velocity fluctuations measured at the centreline of the forward velocity stream in the exit plane; the signals were low-pass filtered below 8 kHz. The speed controller provides steady operation over long time intervals. The mean and fluctuating quantities vary by less than 2% over periods on the order of one hour or more; temperature variations of less than 1 °C were maintained over comparable time intervals by room air conditioning.

The reverse flow stream U_2 is provided by a constant-speed Fuji regenerative blower/suction pump. The reverse flow rate is throttled with a bleed valve in the line connecting the 16-port manifold to the pump. A long settling tube of 3 m in length

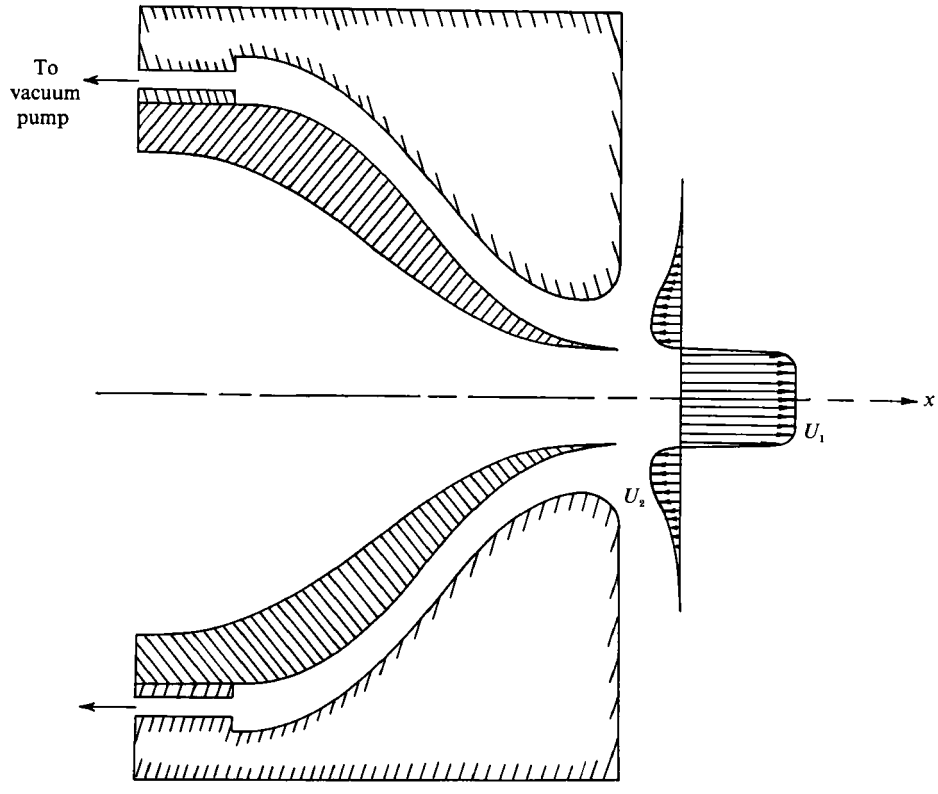

FIGURE 2. Nozzle configuration used to generate an axisymmetric countercurrent mixing layer. The forward stream U_1 and the reverse stream U_2 are defined in a coordinate system with its origin in the nozzle exit plane.

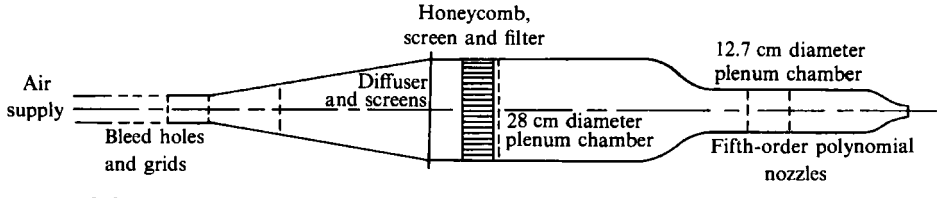

FIGURE 3. Schematic of the low-turbulence test facility used to generate the forward velocity stream U_1. The air exhausts into the laboratory from a circular nozzle having an exit diameter of 2.54 cm; the total system is 6 m in length. The drawing is not to scale.

is used to isolate pump pulsation from the nozzle manifold. Care is also taken to ensure that the volume flow through each of the 16 flexible lines to the nozzle is the same. A hot wire was mounted on a rotary platform to monitor azimuthal variations in the reverse velocity at the inlet to the suction collar. These measurements did not reveal any azimuthal undulations caused by the 16 suction ports. The entire pump is housed within an anechoic chamber to minimize the acoustic level in the laboratory.

Acoustic coupling between the blower-blade passage frequency and tunnel resonance modes exists at certain blower speeds and influences not only the overall turbulence level but also provides discrete forcing of the jet shear layers and jet

column. These effects can be effectively eliminated at any desired forward flow velocity by opening a larger number of holes in the section upstream of the diffuser or by adding resistive elements such as grids to alter the blower operating point. To avoid some of these difficulties we fixed the forward velocity in all of the experiments at $U_1 = 2000$ cm/s – a Reynolds number based on the jet diameter D of $Re_D = 34000$ – and varied the velocity ratio R by altering the magnitude of the reverse flow stream U_2. (An exception to this will be made in §§6.2 and 6.3, where lower forward velocities were used to study curvature effects and to accommodate flow visualization.) A forward velocity of 2000 cm/s was selected for two reasons. First, volume flow restrictions of our suction pump and manifold prevented suction velocities greater than $|U_2| = 430$ cm/s, allowing a study of countercurrent mixing up to an upper limit of $R \approx 1.5$. Second, we wanted to minimize shear-layer curvature effects so our results could be compared with the spatio-temporal stability theory of plane mixing layers (Huerre & Monkewitz 1985). Michalke (1971) suggested that curvature effects could be neglected if the shear-layer momentum thickness was less than approximately $D/50$, although the work of Drubka & Nagib (1981) and Kibens (1989) indicates that a thinner shear layer, on the order of $D/240$, is necessary to eliminate the coupling between the shear layer and jet column instabilities. The exit momentum thickness from the forward stream at $U_1 = 2000$ cm/s was equal to approximately $D/230$ downstream of the jet exit. When suction is applied, the total momentum thickness increases slightly but still is sufficiently small that curvature effects can be neglected. Measurements of the momentum thickness are given in §4; a study of the influence of curvature can be found in §6.2.

3.2. *Instrumentation and probe orientation*

All velocity measurements were made with Dantec 55M-series hot-wire anemometers and 5 μ-hot-wires etched to a working length of 1.25 mm. The hot-wire voltage records were filtered and amplified with a Krohn-Hite model 3343 signal conditioner before being digitized on a Keithley 1944A 16-bit voltmeter; final data processing including linearization was performed on an Everex Step 386 workstation. Power spectra of the streamwise velocity fluctuations were Bartlett-averaged over 32 records of 1024 points giving a resolution of approximately 16 Hz; the typical shear layer instability frequency was of the order of 2000 Hz.

Hot wires – stationary in the reference frame of the nozzle – were employed to measure mean and fluctuating velocities in the jet. The presence of forward and reverse flow limited the placement of the hot-wire probes and supports to minimize probe interference effects. With the exception of shear-layer mean velocity profiles, the data were gathered with hot wires positioned in the forward velocity stream and supports aligned with the jet axis. (All supporting structure was positioned outside the jet shear layers and care was taken to minimize the vibration of the sensing hot wire.) The shear-layer data were gathered on the high-speed of the layer at the non-dimensional locations of $(u-\bar{U})/\Delta U = 0.1$ and 0.4; u is the local time-averaged velocity. Interference effects resulting from the probe supports in the high-speed side of the mixing layer were carefully examined. The band of unstable frequencies in the shear layer displayed no discontinuous behaviour in the axial direction, indicating that the shear-layer tone phenomenon described by Hussain & Zaman (1978) was not significant in these studies.

Mean velocity data were acquired to define the jet velocity ratio and compute the momentum thickness of the shear layer. Obtaining the mean velocity required the hot-wire probe to be oriented to distinguished between both the forward and reverse

velocities by relying on the rectifying effect of the hot wire. This was accomplished by aligning the hot-wire probe support in the radial direction; i.e. perpendicular to the jet axis. The directional sensitivity of the hot wire depends on its geometric symmetry, the orientation of the wire to the flow stream, and temperature differences between the forward and suction streams. The hot-wire sensors were carefully aligned to be parallel to the nozzle face and were calibrated in both directions by simply rotating the probe in its support housing. Our experience with commercially available Dantec probes suggested that the geometric irregularities were indeed small and resulted in virtually identical calibrations in both orientations. Given the uncertainty introduced by the flow around the probe supports, which was causing both flow acceleration and vortex shedding, the errors introduced by geometric asymmetry were, no doubt, insignificant. An approximation of measurement errors was made by comparing the momentum thickness measured by hot wires held with probe supports both parallel and perpendicular to the flow stream in a jet without reverse flow. The perpendicular wire consistently overpredicted the momentum thickness by 3 to 4% when compared to the parallel hot wire. Quantifying the uncertainty of such a technique became more ambiguous when suction was applied to the jet, with most of the uncertainty being related to processing of the rectified hot-wire voltages (see §4 for further discussion). Temperature variations between the jet core and the surrounding ambient fluid, which made up the reverse flow stream, were measured to be less than 0.5 °C, and, therefore, no temperature correction was applied to the hot-wire voltages.

4. Mean velocity field

4.1. *'Standard' jets*

Mean velocity profiles were taken in a 'standard' jet (without reverse flow; $R = 1$) to determine the streamwise self-similarity of thc shear layer generated using the fifth-order nozzle contraction. All mean velocity shear-layer profiles were non-dimensionalized in the coordinates $(u-\bar{U})/\Delta U$ and $(y-y_{0.5})/2\theta$, y being the radial direction and $y_{0.5}$ the position in the shear layer where $u = \bar{U}$. The momentum thickness θ was computed from the equation

$$\theta = \int_{y_L}^{\infty} \left(\frac{1}{4} - \left(\frac{u-\bar{U}}{\Delta U} \right)^2 \right) \mathrm{d}y, \tag{4.1}$$

where the lower limit of integration, y_L, was chosen to minimize uncertainties caused by very low velocities in the standard jet ($R = 1$), the presence of a sizeable radial velocity component, and velocity rectification in jets with reverse flow ($R > 1$); y_L represents the radial position where $(u-\bar{U})/\Delta U = -0.4$. We observed a 4% velocity overshoot at the shoulder of the jet, which was anticipated with the fifth-order polynomial nozzles used and is consistent with the findings of Tan-Atichat (1980) and Drubka & Nagib (1981); the maximum velocity was used to normalize the mixing layer on the high-speed side. Figure 4 indicates that the mean velocity field for a jet with $R = 1$ is self-similar for distances downstream of the nozzle greater than approximately $x/D = 0.079$. Upstream of $x/D = 0.079$, the wake effect of the nozzle lip causes a rapid departure from self-similarity, as evidenced by the profile at $x/D = 0.02$. We have defined the initial momentum thickness θ_0 of the jet shear layer as the value measured at $x/D = 0.079$ ($x = 2$ mm). This definition of θ_0, while somewhat arbitrary, corresponds approximately to the most upstream position where the band of unstable shear-layer frequencies rises above the background level;

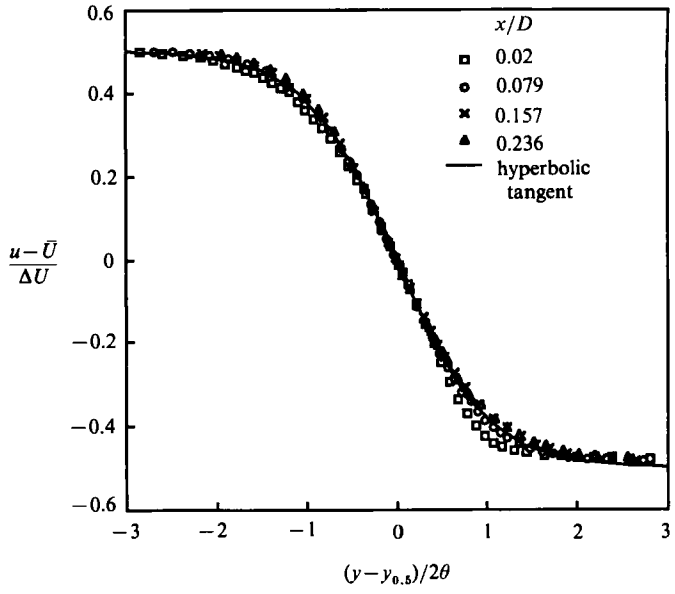

FIGURE 4. Normalized mean velocity profiles in a standard jet mixing layer ($R = 1$). The jet forward velocity $U_1 = 2000$ cm/s.

this is precisely the location that Drubka & Nagib (1981) claim to be most relevant in scaling the dynamics of the initial mixing layer. One further consideration leads us to this operational definition. For velocity ratios greater than unity, the measurement of the velocity profiles upstream of $x/D = 0.079$ becomes more difficult owing to geometric constraints imposed by the probe shaft alignment perpendicular to the jet axis.

Husain & Hussain (1979), Drubka & Nagib (1981), Drubka, Reisenthel & Nagib (1989), and others have shown that the initial conditions of the boundary layers exiting the nozzle significantly influence the spatial development of the jet shear layer and jet column. In all facilities one must establish whether the exit boundary layers are laminar or turbulent and, in particular, determine the distribution of the mean and fluctuating quantities across the boundary layer. In the present study, it was not possible to accurately measure these quantities inside the nozzle because the exit diameter was quite small. Based on indirect measurements made in the shear layers downstream of the nozzle, we concluded that our exiting boundary layer was laminar. The initial momentum thickness θ_0 measured in the separated layer at a velocity ratio of unity was inversely proportional to $Re_D^{\frac{1}{2}}$, which was the anticipated laminar dependence; a least-squares fit to the data produced the expression $\theta_0/D = 0.707 Re_D^{-\frac{1}{2}} + 0.000427$. In addition, a hot wire was inserted into the nozzle boundary layer to estimate the peak level of the velocity fluctuations. The measured maximum intensity of $u'/U_1 \approx 0.015$ was consistent with the values obtained by Drubka & Nagib (1981) in jets having laminar boundary layers with comparable core turbulence intensities; u' represents the r.m.s. intensity of the streamwise velocity fluctuations. Further confirmation that the exiting boundary layers are laminar is provided by spatial growth rate data gathered in the shear layer of a standard jet. The spatial growth rates of the fundamental – the fundamental mode refers to the initial, axisymmetric shear layer instability – and subharmonic compare favourably with the spatial linear stability theory of a Blasius shear layer (to be presented in §5).

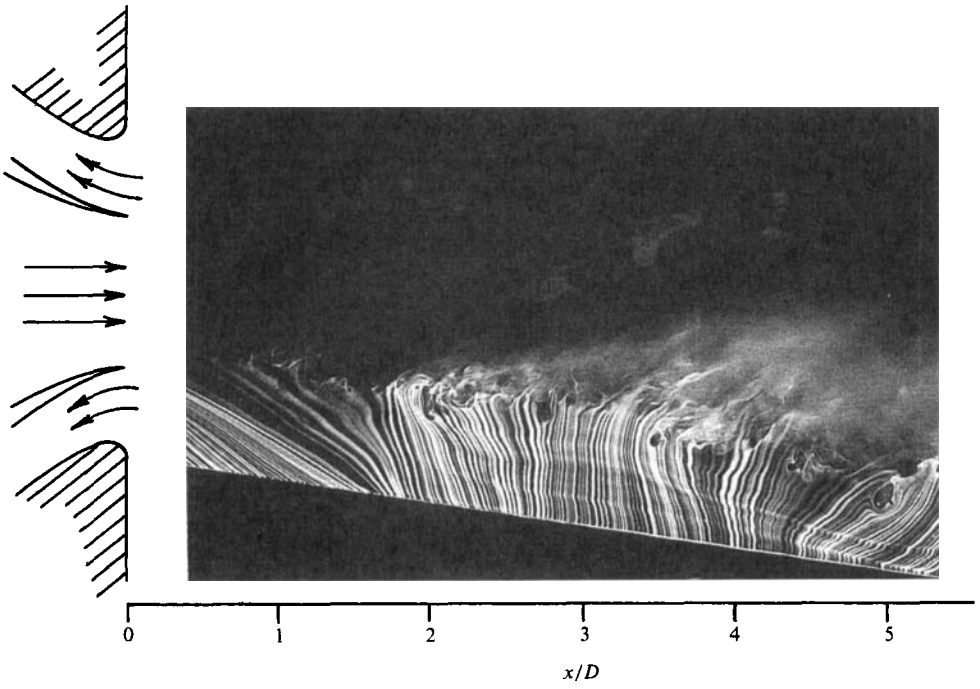

FIGURE 5. Smoke-wire flow visualization of the fluid entrained into the jet at $R = 1.5$ and $U_1 = 2000$ cm/s. Countercurrent mixing can be established in the shear layer for streamwise distances up to $x/D = \approx 3$.

4.2. *Counterflowing jets*

Mean velocity profiles were measured in the jet shear layers for velocity ratios from $R = 1.1$ to 1.5 to obtain the momentum thickness θ_0. These data were gathered by processing hot-wire voltage signals obtained with a probe held perpendicular to the flow. Owing to the rectifying effect of the hot wire, a local-minimum velocity was observed which could be used to distinguish between forward and reverse velocities in the shear layer. Refinement of the velocity profile, resulting in the removal of some data points, is somewhat subjective but is necessary to obtain consistent estimates for the momentum thickness. The removal of data from the profile was based on the criterion that the integrand of equation (4.1) varies smoothly; in particular the function was examined for unusual 'bumps' and 'discontinuities'. After ambiguous data were removed, the integrand of (4.1) was fitted with cubic spline and integrated. The data were closely approximated by the expression $\theta_0/D = 0.009\,14 - 0.004\,84R^{-\frac{1}{2}}$ ($1 \leqslant R \leqslant 1.5$; $U_1 = 2000$ cm/s), which was used to normalize all subsequent data. (The reader is referred to the thesis of Niccum 1990 for a more detailed description of the measurements.)

Before we proceed, several points must be made concerning the nature of the countercurrent mixing layer which is under investigation. Until now we have implicitly assumed that a spatially developing countercurrent mixing region can be generated by applying suction to the jet, and that the mixing region can be represented by a fixed value of the velocity ratio R. To the contrary, our intuition suggests that for large downstream distances the air entrainment into the jet forward stream will be from the ambient air and not from the reverse flow stream, suggesting

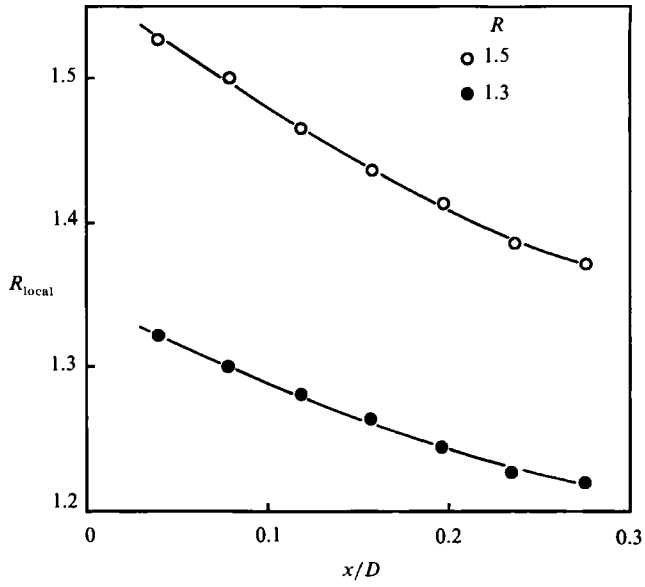

FIGURE 6. Variations in the local velocity ratio downstream of the nozzle exit. The reference velocity ratio R is defined as the local velocity ratio measured at $x/D = 0.079$.

that the flow downstream must approach the conditions of a standard jet with a local velocity ratio of unity. Furthermore, if the entrained flow travels upstream near the nozzle and downstream in the far field of the jet, there must exist a free-stagnation region somewhere in between.

In an attempt to identify such a region and elucidate the flow acceleration near the nozzle, we employed the entrainment smoke-wire technique described by Drubka & Nagib (1981). A fine stainless-steel wire (of diameter 0.13 mm) was anchored at the nozzle face at a radial distance of 3 cm from the jet centre (5 mm outside the suction slot). The wire was held in the axial plane and at an angle to the jet centreline greater than the spread rate of the jet. The wire was wiped with Shell Rimula-30 oil before each run and a voltage was applied to vaporize the oil and mark the entrained fluid. The resulting smoke streaklines are shown in figure 5 for a velocity ratio of 1.5. It is clear that the entrained fluid is drawn upstream into the suction slot only near the nozzle. Farther downstream the streaklines indicate the formation of a stagnation region at $x/D \approx 3$, which is followed still farther downstream by fluid entrainment from the ambient air. This qualitative behaviour was confirmed by the placement of the entrainment wire at other radial positions. The smoke-wire technique proved to be of little help in identifying vortical structures in the shear layer because the forward velocity (20 m/s) was so high. We will examine these structures in more detail at a lower jet velocity in §6.3.

Figure 5 shows that the local velocity ratio of the jet mixing layers, R_{local}, must be a function of the axial position x. The actual spatial dependence was obtained by traversing a hot wire in the axial direction at a fixed radial position corresponding to the centre of the suction slot. Figure 6 reveals that R_{local} decreased monotonically, indicating an acceleration of the reverse flow as it approached the nozzle. We defined the reference velocity ratio R of the jet as that value measured at our reference station $x/D = 0.079$ (R will be used without the subscript 0 for convenience). This definition was attractive not only because it is consistent with our reference station

for evaluating θ_0, it is also physically appealing for the following reason. As we will show in §5 (see e.g. figure 11), the streamwise velocity fluctuations in the jet shear layer display a well-defined exponential growth over the non-dimensional distance of $Rx/\lambda = 2$ before becoming saturated. (λ is the wavelength of the naturally occurring axisymmetric mode, i.e. fundamental, immediately downstream of the nozzle and was computed from the relation $\lambda = \bar{U}/f$, where f is the frequency of the fundamental.) To compare our results to linear stability theory (Monkewitz & Huerre 1982; Huerre & Monkewitz 1985) we selected an average value of R_{local} over this spatial distance. Using as an example the data from figure 6 at $R = 1.5$, we found that over this distance ($0 \leqslant x/D \leqslant 0.17$) the local velocity ratio varied between $1.43 \leqslant R_{\text{local}} \leqslant 1.56$ or an average value of 1.495. Therefore, the reference velocity ratio of $R = 1.5$ corresponds approximately to the centre of the region of well-defined exponential growth. At different velocity ratios a similar behaviour was found; for $R = 1.3$, from figure 6, the average velocity ratio over two disturbance wavelengths was 1.29. In all cases R_{local} varied by approximately $\pm 5\%$ of R in the region of exponential growth of the fundamental. Although this approach was found to provide satisfactory results in the present study where R was varied between 1 and 1.5, it will lead to greater uncertainty for more disparate values of R, because the centre of the exponential region varies in the axial direction. Finally, in addition to selecting a representative velocity ratio at $x/D = 0.079$ we will use this position to define values of $\bar{U}$ and ΔU, which will be necessary for subsequent velocity normalization.

5. Shear-layer evolution

5.1. *Preliminary observations*

The streamwise velocity fluctuations in the shear layer and core of the counterflowing jet were measured for velocity ratios between $R = 1$ and 1.5. As the velocity ratio of the jet was increased, we observed a transition at a critical velocity ratio R_{cr}. Although spatial changes were observed continuously as the velocity ratio was varied, the flow changes encountered at R_{cr} were quite dramatic and constitute the central theme of this paper. Anticipating the results to follow, we believe that these changes are associated with an emerging global model which significantly alters the flow character in the shear layers as well as the jet core far downstream.

As an introduction to this phenomenon, we have provided hot-wire voltage records in figure 7 which reveal the changes occurring in the shear layers and core of the jet for the velocity ratios of $R = 1$ and 1.5. In the experiment, a hot-wire probe was fixed in the high-speed side of the mixing layer at $x/D = 0.375$ and recorded the signals given in figure 7 (*a*). The amplitude scales are identical and reflect the basic observation that sufficient suction applied to the shear layers produces extremely energetic shear-layer oscillations. Although these signals were acquired at a fixed spatial position, and therefore do not reflect a proper non-dimensional reference frame for comparison, we can conclude that properly scaled data exhibit a similarly robust character (e.g. figure 13 below). Accompanying the energetic shear-layer oscillations was a substantial suppression of the oscillations in the core of the jet as shown in figure 7 (*b*). This suppression is very similar to that observed by Zaman & Hussain (1981) obtained by acoustically and mechanically exciting the shear layers of a circular jet. Other observations, including changes in the mean velocity and spectral character, corroborate the notion that a global mode emerges in the jet when sufficient suction is applied. However, at this point we postpone any further

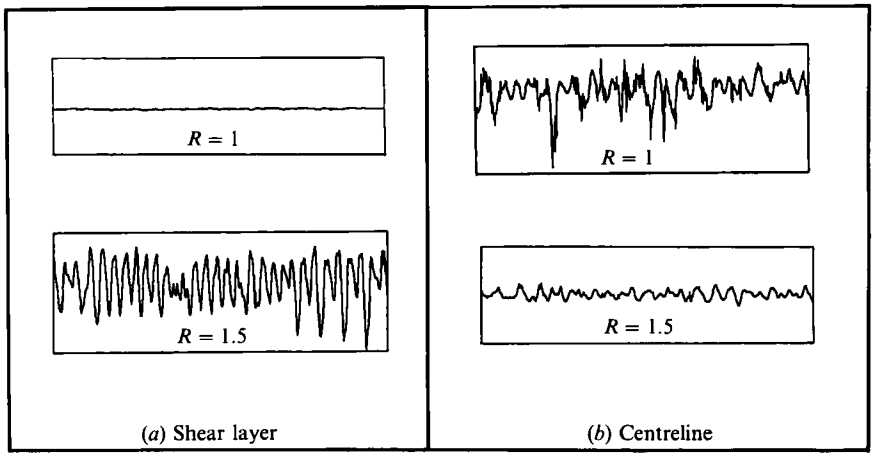

FIGURE 7. Streamwise velocity fluctuations in the jet on (*a*) the high-speed side of the shear layer at $x/D = 0.375$, and (*b*) on the jet centreline at $x/D = 4.0$. The amplitude scales are identical in all four traces but the timescale in (*b*) has been compressed; $U_1 = 2000$ cm/s.

discussion of unstable global modes (until §7) and proceed here to describe some of the basic observations we made in the shear layers of a circular jet with counterflow.

5.2. *Initial shear-layer instability: frequency domain*

Applying suction to the periphery of the jet not only produces energetic oscillations in the shear layers, but also changes the spectral character of the oscillations. A hot wire positioned in the high-speed side of the mixing layer at $x/D = 0.25$ recorded the time series and power spectra given in figure 8; the hot wire was positioned in the radial direction at $(u-\bar{U})/\Delta U = 0.4$. At $R = 1$ there is an unstable band of frequencies centred around 2200 Hz, corresponding to a non-dimensional frequency $f\theta_0/2\bar{U} = 0.012$, which is in agreement with that reported by Freymuth (1966), Hussain & Zaman (1978), Drubka & Nagib (1981), and others for the natural occurring instability of a mixing layer. As the velocity ratio is increased, the time series data (all amplitude scales are equivalent) reveal that the oscillations become quite strong, increasing in r.m.s. intensity by roughly two orders of magnitude from $R = 1$ to 1.5. In addition, there is a transition in the frequency behaviour from an unstable band of frequencies to essentially a 'discrete' frequency between R of 1.3 and 1.4. This observation is quite general and can be verified at all positions in the mixing layer. The power spectrum at $R = 1.5$ shows that the subharmonic dominates the fundamental, a consequence of the fact that at a fixed streamwise position we are seeing more advanced stages of the mixing-layer development.

To properly compare the spectral behaviour in mixing layers having different velocity ratios, we collected a series of data at $(u-\bar{U})/\Delta U = 0.4$ and at a non-dimensional streamwise position of $Rx/\lambda = 2$ (see figure 9). A single peak emerges in the power spectrum near $R = 1.4$ at a frequency of 2500 Hz or $f\theta_0/2\bar{U} = 0.0185$. The discrete frequency behaviour found at $R = 1.4$ is qualitatively similar to power spectra observed in mixing layers subjected to monochromatic excitation (Zaman & Hussain 1980, 1981). The 2500 Hz component, which rises above the background between R of 1.3 and 1.4, can also be observed as a sideband peak at smaller velocity ratios. In an effort to define a critical velocity ratio, the magnitudes of the 2500 and 2200 Hz components were compared by integrating the mean-squared energy over

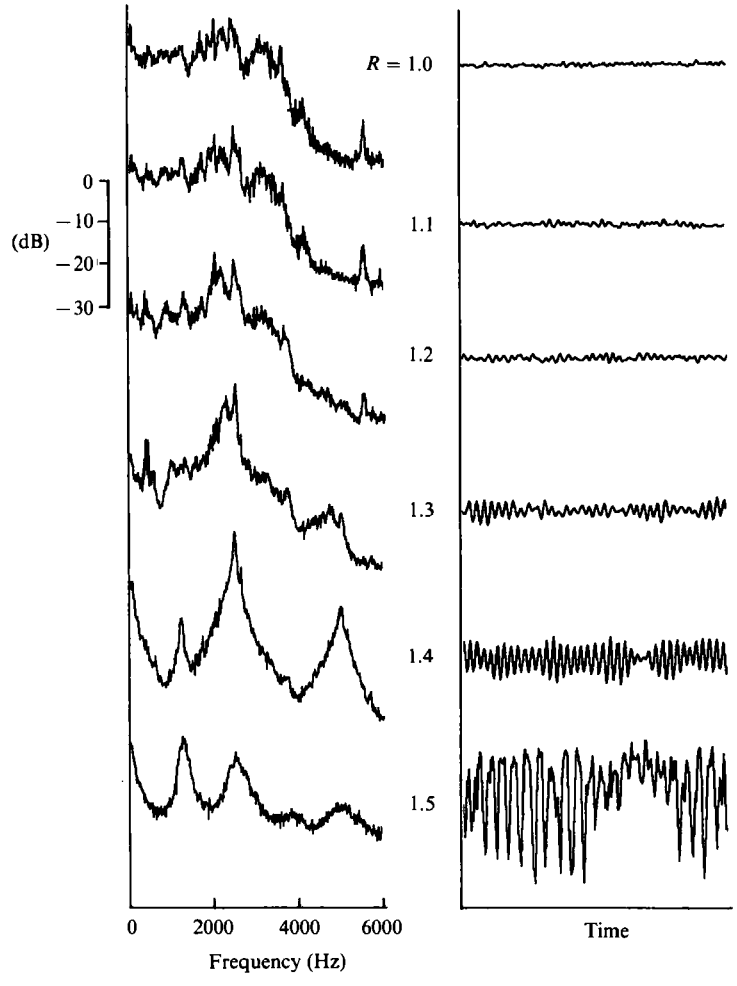

FIGURE 8. Velocity power spectra and corresponding time traces taken in the shear layer at $x/D = 0.25$ and $(u-\bar{U})/\Delta U = 0.4$. The time records have identical amplitude and timescales; $U_1 = 2000$ cm/s.

comparable bandwidths at each frequency. As shown in figure 10(*a*), when the velocity ratio is increased from $R = 1$ to 1.3 the 2200 Hz component increases in relative strength to the sideband frequency at 2500 Hz; however, this trend is abruptly reversed with further elevations in the velocity ratio. An estimation of the critical velocity ratio can be obtained by defining R_{cr} as the value when the sideband frequency first dominates, namely when the ordinate in figure 10(*a*) equals unity; in this fashion we obtain $R_{cr} \approx 1.32$. (The power spectral behaviour is independent of whether the velocity ratio is increased or decreased across R_{cr}, indicating that the phenomenon is not hysteretic.)

The frequency changes accompanying this transition are shown in figure 10(*b*), where the data correspond to the 2200 Hz component for $R < R_{cr}$ and the 2500 Hz component for $R > R_{cr}$. Several points must be made to clarify the nature of the 2200 and 2500 Hz shear-layer oscillations. The amplified disturbances in the subcritical mixing layer (e.g. at $R = 1$ and 1.2 in figure 9) are observed over a wide band of frequencies, the centre of which is at approximately 2200 Hz. The hatched region in

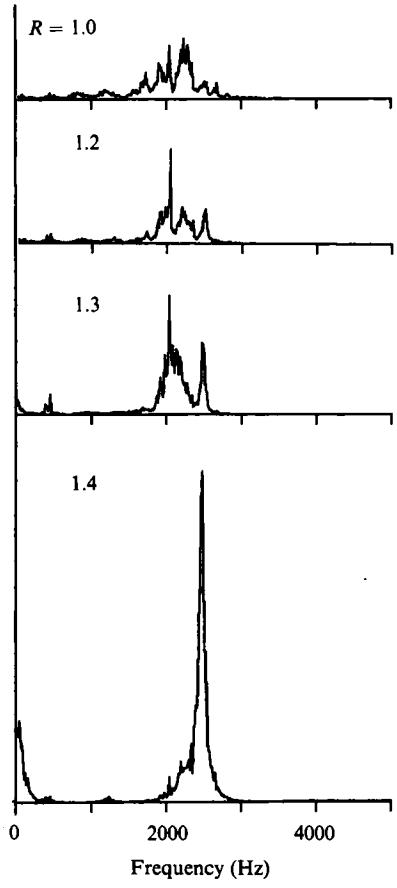

FIGURE 9. Velocity power spectra (linear scale) measured in the shear layer at the non-dimensional position of $Rx/\lambda = 2$ and $(u-\bar{U})/\Delta U = 0.4$. The forward velocity is 2000 cm/s.

figure 10(*b*) illustrates the range of disturbance frequencies that is amplified above the background level. By contrast, the oscillations in the supercritical mixing layer at 2500 Hz are quite 'pure' (e.g. at $R = 1.4$ in figure 9).

A close comparison of the spectral distributions in figure 9 reveals that the 2500 Hz component, which dominates the shear layer at $R = 1.4$, is already present at subcritical velocity ratios. To establish whether the oscillations emerging at R_{cr} are the consequence of a global instability, it is first necessary to rule out the possibility that the oscillations are caused by some discrete forcing specific to our facility, such as a tunnel acoustic mode or a resonance in the suction device. The spectral content of the background turbulence was examined at several locations in the nozzle, between the exit plane and the plenum chamber upstream. Power spectra obtained with and without suction revealed an absence of discrete forcing (above the background turbulence level) at 2500 Hz or its harmonics (see Niccum 1990). We believe, therefore, that the presence of an external forcing frequency is not essential for the formation of the pure spectral peak at R_{cr}.

To test this hypothesis further, we briefly explored the nature of the shear-layer oscillations at an elevated forward velocity, corresponding to $Re_D = 42\,500$. We again observed an unstable band of frequencies at $R = 1$; however, they were centred at 3450 Hz. As the velocity ratio was increased, a pure spectral peak emerged at a

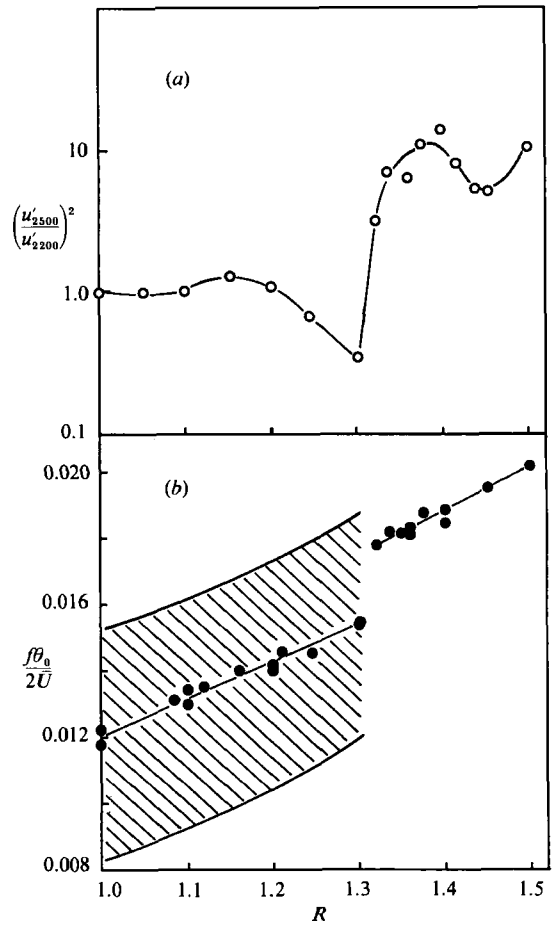

FIGURE 10. (*a*) Ratio of the energy contained in the 2200 and 2500 Hz frequency components at $x/D = 0.25$ and $(u-\bar{U})/\Delta U = 0.4$. (*b*) Range of amplified frequencies in the mixing layer (the fundamental).

frequency of 3750 Hz. The non-dimensional frequency of the subcritical and supercritical oscillations, $f\theta_0/2\bar{U}$, was approximately 0.013 (at $R = 1$) and 0.019 (at $R = 1.4$), respectively, which agree quite well with the scaling found in figure 10(*b*) at $Re_D = 34000$. Furthermore, the 3750 Hz component was not observed as a significant peak in the spectrum at $R = 1$, indicating that background forcing does not play a dominant role in the selection of the spectral peak at R_{cr}. (The strong amplification of the supercritical spectral peak of 2500 Hz at slightly subcritical velocity ratios requires some additional explanation. This will be addressed in §8.)

5.3. *Initial shear-layer instability: spatial domain*

One important aspect of this study was to document the spatial development of mixing layers having velocity ratios greater than unity. As we have already described in §4.2, the velocity ratio varies continuously in the streamwise direction owing to the acceleration of the reverse flow stream as it approaches the nozzle. In fact, the local velocity ratio decreases by approximately 10% in the first two disturbance wavelengths. Despite these difficulties, we compared the spatial growth rates of the fundamental and subharmonic waves in the non-dimensional streamwise

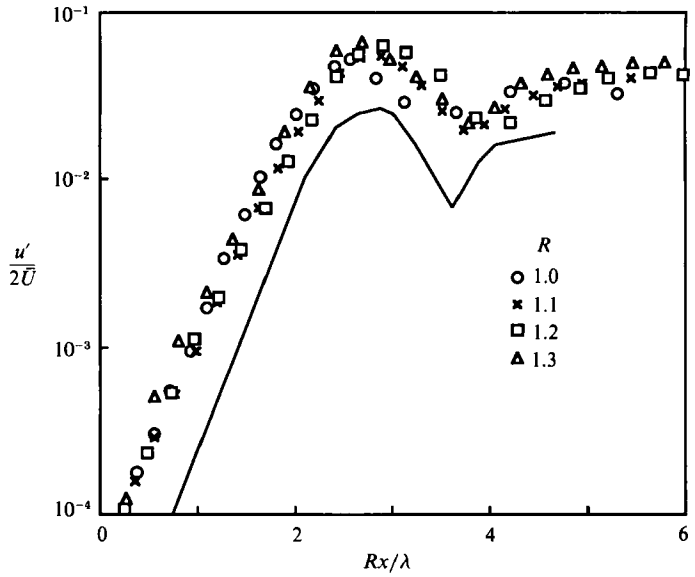

FIGURE 11. Spatial development of the fundamental instability (axisymmetric) mode of the jet. Data were gathered in the shear layer at $(u-\bar{U})/\Delta U = 0.1$. The data of Drubka & Nagib (1981) were gathered at $R = 1$ (——).

coordinate Rx/λ. The reasonable collapse of our data for R between 1 and 1.3 indicates that these streamwise variations are not too significant at least over distances where the linear theory is valid.

The streamwise velocity fluctuations $u'/2\bar{U}$, obtained at velocity ratios from $R = 1$ to 1.3, will be presented first. The radial position of the hot wire was adjusted at each streamwise station to capture the maximum amplitude of the disturbance eigenfunction, which corresponded to $(u-\bar{U})/\Delta U = 0.1$. The spatial growth of the fundamental is plotted in figure 11 for velocity ratios up to 1.3. The data collapse onto a single curve showing both a region of well-defined exponential spatial growth (for $Rx/\lambda < 2$) and the characteristic minimum at $Rx/\lambda \approx 4$. The data taken by Drubka & Nagib (1981) at $R = 1$ are provided for comparison and shows good qualitative agreement with the present experiments. Their data were taken in a facility having a similar fifth-order polynomial jet nozzle at the same initial shear-layer Reynolds number $U_1\theta_0/\nu$ of 150 ($U_1 D/\nu = 34000$). Their exit turbulence intensity of 0.05 % on the jet centreline was lower than that in our facility, but other data taken by Drubka & Nagib indicate that the spatial behaviour will be essentially the same at our turbulence intensity of 0.1 %. (We believe that their curve lies below ours because a narrower bandwidth was used by these authors to isolate the fundamental from the background.)

The spatial growth of the subharmonic wave is given in figure 12 for velocity ratios from 1 to 1.3 together with the results of Drubka & Nagib (1981) for $R = 1$. The two sets of data at $R = 1$ corroborate a region of linear spatial growth followed by a more rapid amplification process coincident with the saturation of the fundamental; the change in amplification rate occurs at $Rx/\lambda = 2$. The subharmonic data taken at different velocity ratios do not collapse as well as the fundamental observed in figure 11, although each displays the characteristic break in slope. A proper normalization of the data would employ the wavelength of the subharmonic, which is dispersive and depends on the spatial variation of the momentum thickness and velocity ratio.

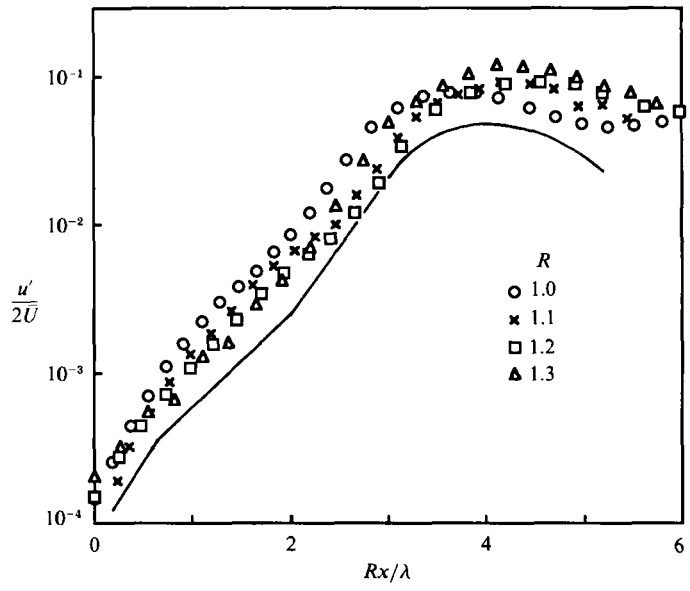

FIGURE 12. Spatial development of the subharmonic instability (axisymmetric) mode of the jet. Data were gathered in the shear layer at $(u-\bar{U})/\Delta U = 0.1$. The data of Drubka & Nagib (1981) were gathered at $R = 1$ (——).

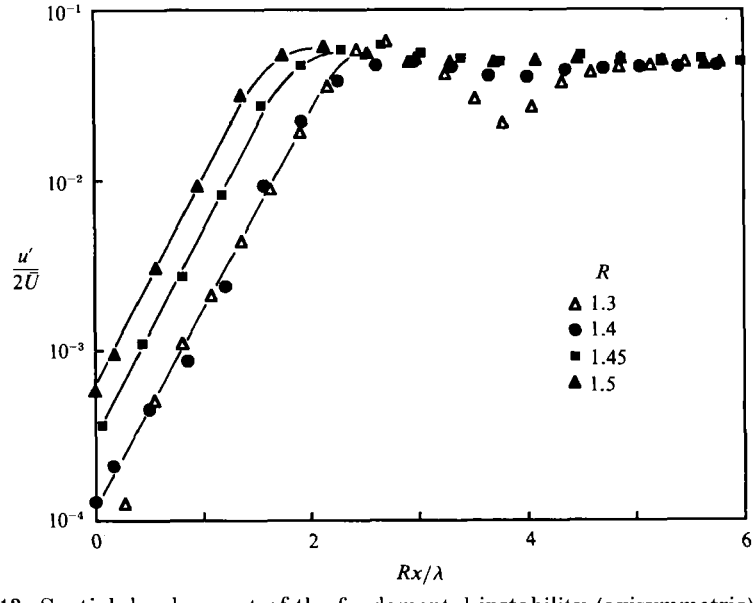

FIGURE 13. Spatial development of the fundamental instability (axisymmetric) mode of the jet. Data were gathered in the shear layer at $(u-\bar{U})/\Delta U = 0.1$.

We now turn our attention to the spatial development of the mixing layer for higher velocity ratios (see figure 13). The spatial growth rate data of the fundamental for $R \geqslant 1.4$ do not collapse in the spatial reference frame Rx/λ, indicating a change in scaling at higher velocity ratios. It would appear that the fundamental amplitude

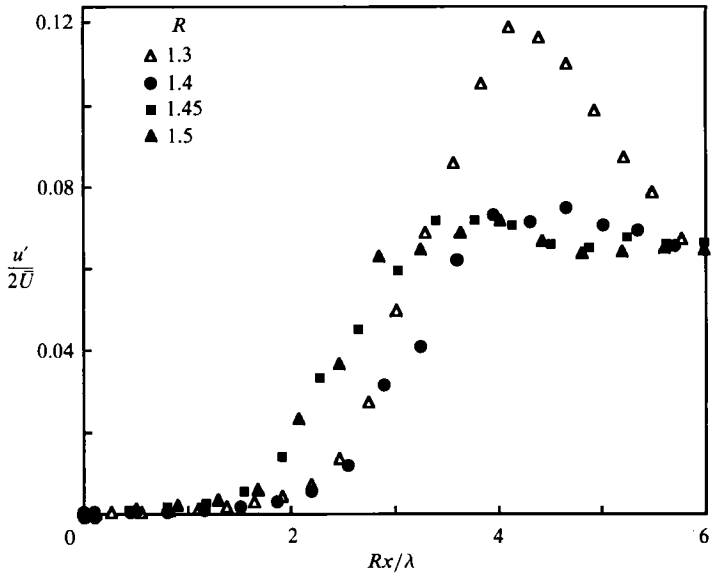

FIGURE 14. Spatial development of the subharmonic instability (axisymmetric) mode of the jet. Data were gathered in the shear layer at $(u-\bar{U})/\Delta U = 0.1$.

saturates at a level which increases with $R-R_{cr}$ (the actual relationship will be investigated in §7). We should point out that the behaviour observed in figure 13 is qualitatively similar to that found by Freymuth (1966) in an axisymmetric mixing layer subjected to different levels of acoustic excitation. When R is increased from 1.3 to 1.4, the amplitude minimum at $Rx/\lambda \approx 4$ is absent, and the amplitude increases by a factor of two. The strong fundamental is a consequence of a more organized vortex motion in the mixing layer, which is reflected in the discrete frequency behaviour shown earlier in figures 8 and 9. Winant & Browand (1974) point out that monochromatic forcing of the shear layer causes less 'jitter' in the spacing of fundamental vortices, which in turn inhibits their amalgamation. Inhibiting vortex pairing will result in a corresponding reduction in the strength of the subharmonic wave in the mixing layer. This suppression can be observed in figure 14 at $Rx/\lambda \approx 4$. A linear amplitude scale was selected to show a twofold reduction in the strength of the subharmonic when R is increased from 1.3 to 1.4.

Next, the appropriateness of the streamwise coordinate Rx/λ needs to be examined. Monkewitz & Huerre (1982) clearly show that the maximum spatial growth rate scales linearly with the velocity ratio for a plane Blasius mixing layer having $R \leqslant 1$; no results are presented for $R > 1$. The findings of Monkewitz & Huerre (1982) together with those of Huerre & Monkewitz (1985) indicate that the maximum spatial growth rate for a hyperbolic tangent profile is not linearly proportional to the velocity ratio for $1 \leqslant R \leqslant 1.3$. Therefore, we rescaled the growth-rate data with $-\alpha_i \theta_0$, instead of R, and obtained an equally satisfying collapse ($-\alpha_i \theta_0$ was taken from our experimental results, where $-\alpha_i$ is the spatial growth rate of the fundamental). We selected the scaling Rx/λ, however, because it appears to be quite suitable in the present problem, as indicated by the collapse of data in figure 11, and because it allows a direct comparison to the existing literature.

We conclude this section by comparing the fundamental and subharmonic growth rates to the spatial linear stability theory. The fundamental growth rates are

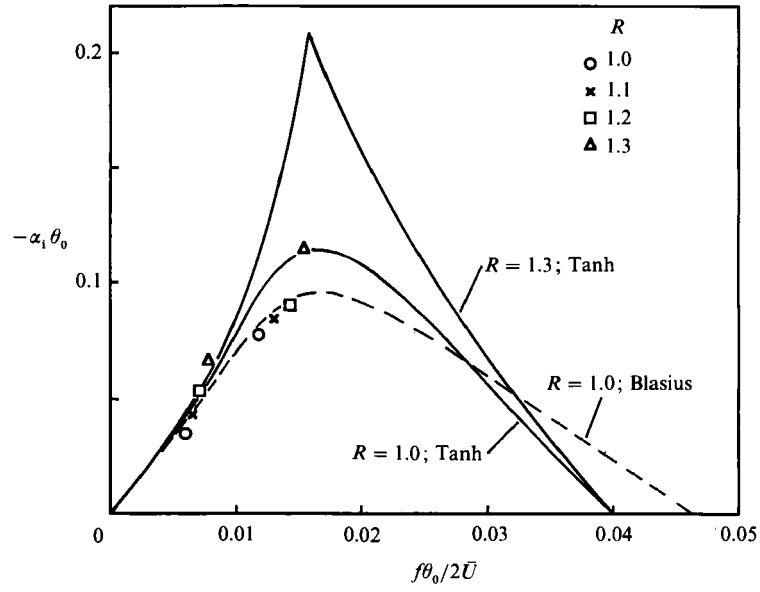

FIGURE 15. Non-dimensional spatial growth rates of the fundamental and subharmonic axisymmetric shear-layer instabilities (f in this figure refers to both the fundamental and subharmonic frequencies). The theoretical results at $R = 1.0$ and 1.3 were taken respectively from Monkewitz & Huerre (1982) and Huerre & Monkewitz (1985).

obtained by performing a least-squares fit to the data having an amplitude below $u'/2\bar{U} = 0.01$. Owing to the multiple slopes present in the subharmonic data, those growth rates are measured directly from log-linear plots. The growth rates taken at R between 1 and 1.3 are given in figure 15 together with the theoretical results of Monkewitz & Huerre (1982) and Huerre & Monkewitz (1985). Our measured growth rates at $R = 1$ fall slightly below the theoretical curve for a Blasius shear layer but are within the uncertainty displayed by other authors (Freymuth 1966; Drubka & Nagib 1981). The experimental data at velocity ratios greater than unity display growth rates significantly below the theoretical predictions for a hyperbolic-tangent shear layer; however, the upward trend with increasing R is borne out satisfactorily. Clearly more theoretical work is needed here – in particular for a Blasius profile at elevated velocity ratios. We are hesitant to draw more detailed conclusions because we do not know the precise shape of the shear-layer profiles in the presence of counterflow. The magnitude of the velocity gradient in the layer can significantly influence the growth rate, as shown by Monkewitz & Huerre (1982). In the presence of reverse flow, a non-intrusive measurement such as a LDV would be necessary to obtain the detailed profile shapes.

One final point can be made regarding the frequency selection in figure 15. As the velocity ratio approaches R_{cr} (from below), the most unstable frequency shifts toward the one having the maximum spatial amplification rate. Zaman & Hussain (1981) showed that monochromatic excitation at the frequency with a maximum spatial amplification rate will lead to a premature saturation of the shear layer and a corresponding suppression of turbulence in the core of the jet. It is precisely this phenomenon which we will explore in the next section.

6. Jet column response

6.1. *Basic observations*

The jet dynamics are complicated by the presence of two lengthscales: the shear-layer thickness and the jet diameter. The sensitivity of the jet at the larger of these two scales was demonstrated by Crow & Champagne (1971), where acoustic forcing was used to excite the column mode of the jet. The development of the jet column is highly dependent on the initial conditions imposed upstream in the separated shear layers. When the separating boundary layer is turbulent, Husain & Hussain (1979) and Raman, Zaman & Rice (1989) observed a lower spreading rate of the shear layer as compared to the laminar case, which resulted in a slower decay of the mean velocity on the jet centreline downstream of the potential core. Similar effects were reported by Drubka & Nagib (1981) for turbulent as well as highly disturbed, laminar, separating boundary layers. Reductions in the mean velocity decay rate and suppression of the jet core turbulence were obtained by Zaman & Hussain (1981) by exciting the jet shear layers near their spatially most unstable frequency. We showed in §5 (e.g. figure 7) that the energetic shear-layer oscillations give rise to a suppression of turbulence in the jet core. In this section we will take a more detailed look at the response of the jet column to the initial conditions imposed by applying suction to the jet shear layers.

The r.m.s. intensity of the streamwise velocity fluctuations on the jet centreline, u'_{c1}, is plotted in figure 16. The data at $R = 1$ are in reasonable agreement with the results of Zaman & Hussain (1981), which were taken in an unforced 2.54 cm diameter jet at a slightly lower Reynolds number of $Re_D = 21400$. The axial variation of the velocity fluctuations remains essentially invariant with velocity ratios from $R = 1$ to 1.3. Between $R = 1.3$ and 1.4, the turbulence level drops over the streamwise distance of $0 \leqslant x/D \leqslant 8$ and is coincident with the emergence of the energetic shear-layer oscillations. Zaman & Hussain obtained a comparable suppression effect by exciting (both acoustically and mechanically) the shear layer at a frequency $f\theta_0/2\bar{U} = 0.017$; these data have been included in figure 16. The similarity between the data at high velocity ratios and those obtained by Zaman & Hussain with monochromatic forcing suggests that the shear layers are self-excited when sufficient reverse flow is applied to the jet shear layers. It is unclear why the suppression effect in the counterflowing jet is not as pronounced as in forced jets. The frequency of the shear-layer oscillations at velocity ratios from 1.4 and 1.5 lies in the neighbourhood of $f\theta_0/2\bar{U}$ of 0.020 (see figure 10), which is within the range of optimal suppression frequencies (0.016 to 0.022) reported by Zaman & Hussain. The reduced suppression in the present problem could be related to an equivalently lower forcing level imposed by the self-excited shear-layer oscillations, although we believe that this is not the case (see discussion below regarding figure 18). Zaman & Hussain showed that the suppression effect depends on the forcing amplitude only at very low excitation levels. However, a close examination of their data (figure 6*b* from Zaman & Hussain) reveals that, although the suppression effect is optimized at $f\theta_0/2\bar{U} = 0.017$, it is also a strong function of the dimensional frequency. This would translate into a dependence on θ_0/D, indicating that the suppression is enhanced by the coupling between the shear layer and jet column modes. We have qualitatively observed some dependence of the suppression effect on θ_0/D in counterflowing jets, but these results are quite preliminary and are best postponed to a later time.

The centreline mean velocity is given in figure 17 together with the excited and unexcited data from Zaman & Hussain (1981). We again observe that the jet column

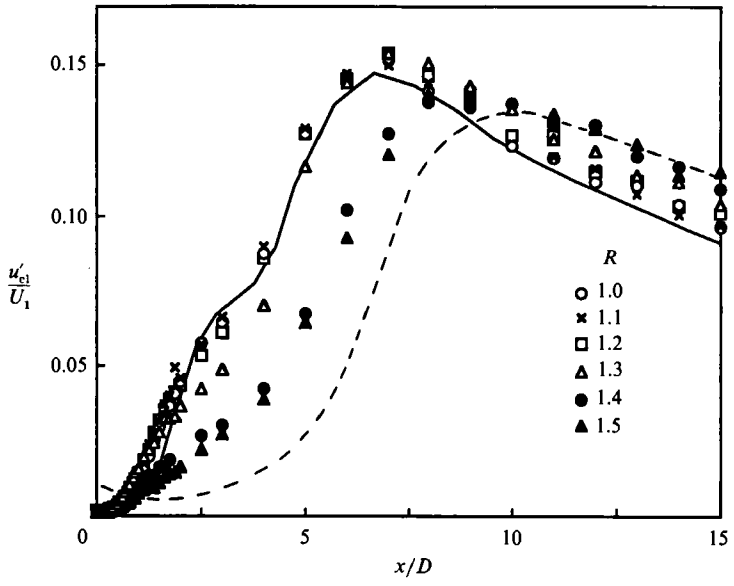

FIGURE 16. The r.m.s. intensity of the streamwise velocity fluctuations on the jet centreline. Data taken in a 2.54 cm diameter jet by Zaman & Hussain (1981) in a jet forced at $f\theta_0/2\bar{U} = 0.017$ (------), and an unforced jet (——) have been included for comparison.

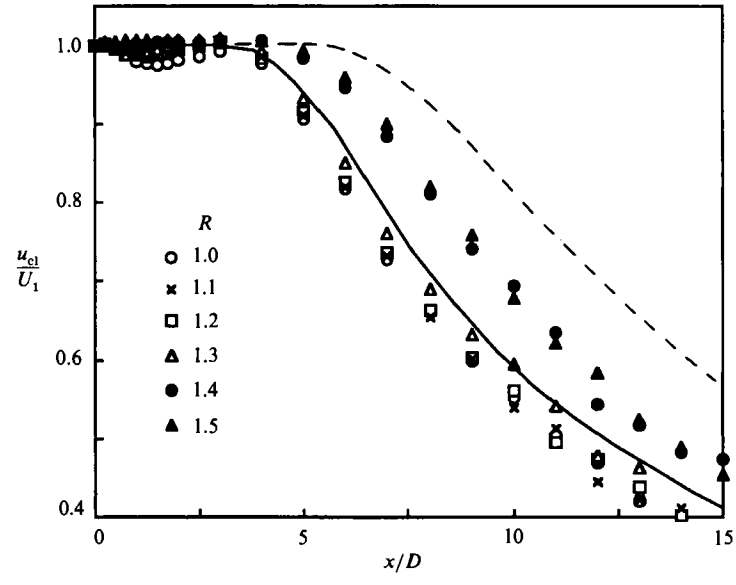

FIGURE 17. The mean streamwise velocity on the jet centreline. Data taken in a 2.54 cm diameter jet by Zaman & Hussain (1981) in a jet forced at $f\theta_0/2\bar{U} = 0.017$ (------), and an unforced jet (——) have been included for comparison.

response falls onto two separate curves depending on the level of excitation in the shear layers. The decay rate of the mean velocity in the present facility at $R = 1$ is more rapid than that reported by Zaman & Hussain. This discrepancy is due to a higher background turbulence intensity in the jet exit plane employed by those

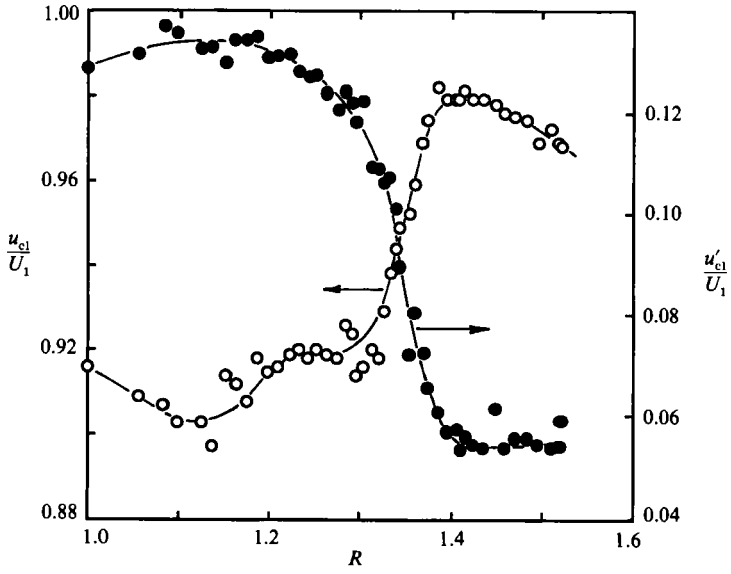

FIGURE 18. Mean and fluctuating velocities measured on the jet centreline at $x/D = 5$ and $U_1 = 2000$ cm/s. The critical velocity ratio is estimated as $R_{cr} = 1.32$.

authors (0.25% compared to 0.1% in the present facility) and is consistent with trends reported by Drubka & Nagib (1981). Drubka & Nagib also reported that the decay rate decreased as the turbulence intensity increased in the shear layer. This trend is very weak in our jet for R between 1 and 1.3 but is quite clearly supported during the transition from R of 1.3 to 1.4 as a consequence of the self-excited shear-layer oscillations.

Figure 17 shows that a transition occurs at a critical velocity ratio R_{cr} between $R = 1.3$ and 1.4. To obtain a more accurate estimate of R_{cr}, we measured the mean and fluctuating velocities on the jet centreline as a function of the velocity ratio (see figure 18). The abrupt rise in the mean velocity provides the sharpest and most reproducible estimation of the onset of the instability producing $R_{cr} = 1.32$, which is consistent with the prediction of R_{cr} obtained from the shear-layer data (figure 10). Note that the dynamics of the jet core are essentially insensitive to reverse flow both above and below the transition. For subcritical velocity ratios ($R < R_{cr}$), the mean properties of the jet change very little, even though the maximum spatial growth rate of the shear layer increases approximately linearly with R. Evidently, the transition is not the consequence of elevated spatial growth rates alone. The insensitivity of the jet at supercritical velocity ratios ($R > R_{cr}$) corroborates the findings of Zaman & Hussain (1981) that the suppression effect is essentially independent of forcing level. (Recall from figure 13 that the amplitude in the shear layer – and therefore the effective forcing level – increases with R.)

6.2. *Influence of jet curvature*

The momentum thickness of the jet shear layer is initially a small fraction of the jet diameter ($D/\theta_0 = 230$ and 190 for $R = 1$ and 1.5 respectively) for the investigated forward velocity of $U_1 = 2000$ cm/s. We argued in §3.1 that under these conditions the jet curvature could be neglected and direct comparisons could be made to the plane-mixing-layer stability analysis of Huerre & Monkewitz (1985). The suction,

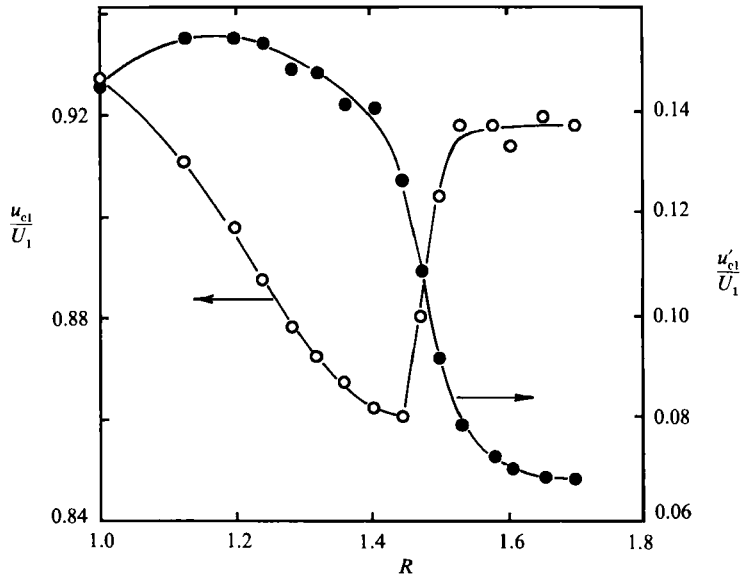

FIGURE 19. Mean and fluctuating velocities measured on the jet centreline at $x/D = 4.5$ and $U_1 = 1000$ cm/s. The critical velocity ratio is estimated as $R_{cr} = 1.45$.

however, influences the shear layer not only as it exits the nozzle but also for several diameters downstream where curvature effects are more significant. (For instance, the momentum thickness increases by 50% in the first one-half jet diameter.) The following study was not exhaustive but was used to determine how the jet curvature might influence the jet behaviour and the prediction of R_{cr}. This was accomplished by varying the forward velocity between 620 and 2000 cm/s (corresponding to D/θ_0 between 135 and 230 for a jet having a velocity ratio of unity) and measuring the mean and fluctuating velocities on the jet centreline. Figure 19 shows that the transition at $U_1 = 1000$ cm/s occurs at $R_{cr} = 1.45$ (defined at the abrupt increase in the mean velocity) in contrast to a value of $R_{cr} = 1.32$ at $U_1 = 2000$ cm/s. The relationship between forward jet velocity and critical velocity ratio is given in figure 20. It is clear that the jet curvature has some influence on stability even at $U_1 = 2000$ cm/s but is rapidly approaching an asymptotic state for higher velocities, or equivalently, thinner shear layers. (The sigmoidal appearance of the curve in figure 20 suggests that the jet response may be different for thicker shear layers. This interesting behaviour requires further study.)

6.3. *Flow visualization*

When the velocity ratio was elevated above R_{cr} we observed highly energetic oscillations in the jet shear layer, which were associated with sharp spectral peaks, indicating very organized vortex structures. These changes resulted in a suppression of the turbulence level in the jet column as well as a slower decay rate of the centreline mean velocity. In an attempt to visualize these changes, we employed the smoke-wire flow visualization technique (Corke *et al.* 1977), which was described briefly in §4.2. In the present study we were interested in viewing the axial plane of the jet, which required tensioning the stainless-steel wire across the jet exit. We supported the wire in the horizontal plane and manually applied the oil before each run. A vertically supported wire works well when operated as a continuous smoke

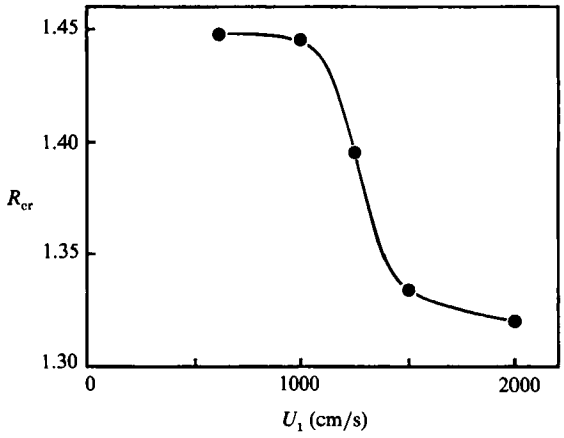

FIGURE 20. The influence of the forward jet velocity (i.e. momentum thickness) on the critical velocity ratio.

wire with an oil reservoir and stroboscope for parametric studies, but we found that a horizontal wire wiped with oil produced the nicest photographs. At a forward velocity of 2000 cm/s, it was possible to mark the reverse flow stream and the shear layer to some extent, but attempts to illuminate smoke streaklines in the jet core proved unsatisfactory. The data presented in §6.2, together with power spectral data, indicate that the general features of the transition that we documented in detail at $U_1 = 2000$ cm/s are present at forward velocities as low as 620 cm/s. We therefore performed flow visualization at $U_1 = 620$ cm/s, where the smoke-wire technique works quite nicely.

The results of the flow visualization study are given in figure 21 for velocity ratios of $R = 1$, 1.2, 1.5, and 1.7; recall from figure 20 that $R_{cr} = 1.45$ at a forward velocity of 620 cm/s. Figure 21 (*a*) shows the axisymmetric vortex ring structure commonly observed in standard jets. The two smaller but distinct vortices (centred at $x/D \approx 1$) in the jet shear layer correspond to a subharmonic disturbance. The coalescence of two such vortices probably resulted in the larger structure observed farther downstream at $x/D \approx 2$; this structure accounts for the spectral energy observed at the quarter harmonic. This general behaviour was consistently observed for velocity ratios up to approximately 1.4. Figure 21 (*b*) indicates that the higher spatial growth rates at $R = 1.2$ produce a slightly larger structure at the same streamwise position when compared to figure 21 (*a*); a vortex pairing is in progress at $x/D \approx 2.5$. Figure 21 (*c*, *d*) reveals the dramatic changes occurring in the jet shear layer and core when the velocity ratio is increased above R_{cr}. There is a noticeable absence of large vortices at supercritical velocity ratios, resulting in minimal pinching of the jet column and, consequently, lower turbulence intensity levels in the jet core (see figure 16). We described the vortices at supercritical velocity ratios as being highly energetic and quite regularly spaced in the streamwise direction. This organized behaviour resulted in saturation of the structures closer to the nozzle, where the transverse scales of the mixing layer limited their growth. This description is consistent with that given by Zaman & Hussain (1981) in an axisymmetric mixing layer forced at the spatially most amplified frequency. These authors predicted that the premature saturation of the vortices prevented them from reaching larger scales farther downstream. This is precisely what we observe at supercritical velocity ratios in figure 21. Since the vortices attain a relatively small scale for $R > R_{cr}$, the spread

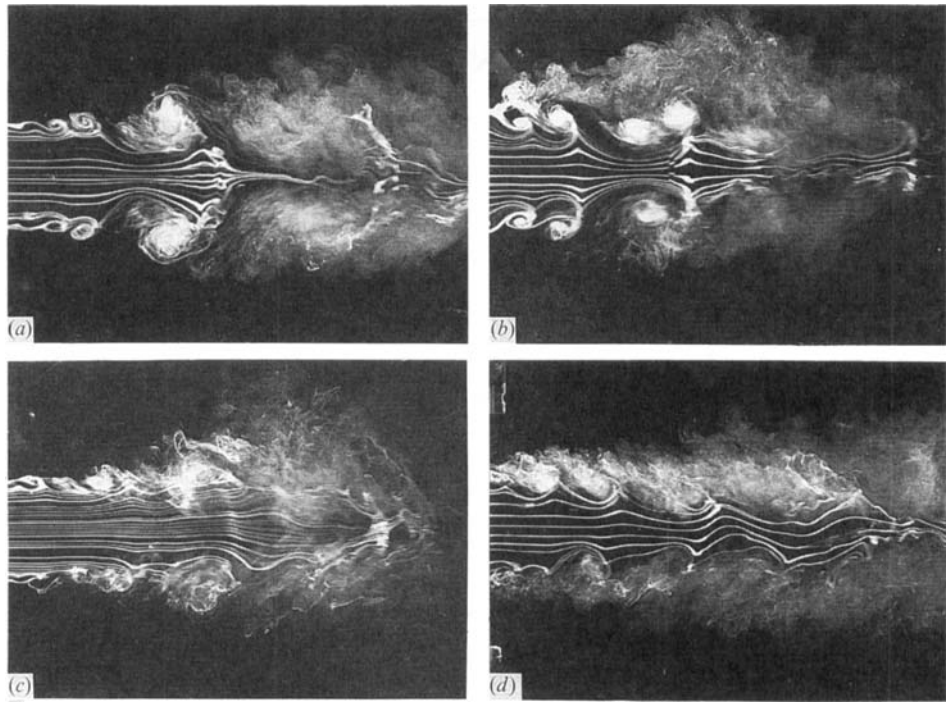

FIGURE 21. Smoke-wire flow visualization of the axial plane of the jet at (*a*) $R = 1.0$, (*b*) 1.2, (*c*) 1.5, and (*d*) 1.7; the forward velocity $U_1 = 620$ cm/s and $R_{cr} = 1.45$. The smoke wire was positioned across the diametral plane of the jet at $x/D = 0.25$. The photographs extend from $0.5 \leqslant x/D \leqslant 5$.

rate of the mixing layer is reduced, and we expect a reduction in the decay rate of the mean velocity on the jet centreline.

Several comments should be made regarding the flow visualization described above. The frequency discontinuity in figure 10 (corresponding to dual peaks in figure 9 at, for instance, $R = 1.3$) represents a frequency rise of 15%. This is about the difference between the axisymmetric and helical mode frequency observed in the low-turbulence jet of Drubka & Nagib (1981). We anticipated that the supercritical mode might correspond to a helical instability, but this was not supported by our flow visualization. In over 150 photographs taken between $R = 1$ and 1.8 we consistently observed the fundamental and subharmonic instabilities of the jet to be the axisymmetric mode. (This does not include the non-axisymmetric behaviour which is sometimes seen farther downstream, such as in figure 21*d*.) We recorded five cases out of 150 ($\approx 3\%$) which were clearly helical in nature, indicating that this mode plays a minor role in the present problem. Finally, we wanted to rule out the possibility that the placement of the smoke wire might have influenced the interpretation of the photographs. If an unstable global mode is responsible for the supercritical jet response, the placement of the smoke wire could possibly alter the stability of the flow significantly. Several authors have reported such behaviour in the supercritical wake (Strykowski & Sreenivasan 1990) and the heated jet (Sreenivasan *et al.* 1989; Monkewitz *et al.* 1990). We carefully traversed our smoke wire in the near field of the jet ($0 \leqslant x/D \leqslant 1$) while recording the flow response at several positions downstream; this was done for both heated and unheated wires. Examination of spectral records, and mean and fluctuating velocities indicates that the wire placement does not affect the jet dynamics in any measurable way. We do

not rule out, however, the possibility that a larger diameter wire positioned in some fashion might alter the jet stability, e.g. an azimuthal ring positioned in the shear layer. This issue requires further study.

7. Global jet stability

In a recent review, Huerre & Monkewitz (1990) described the available experimental evidence of global instability as being obtained from two classes of experiments. The first group of 'easy' experiments examined the stationary behaviour (unsteady but time invariant in the mean) of the flow and provides various forms of circumstantial evidence of global instability. By contrast, the 'hard' experiments included a transient analysis of the bifurcation and furnished conclusive proof that a global mode had emerged. In all cases a control parameter such as the flow Reynolds number, density ratio, or base-bleed coefficient was varied in the neighbourhood of the bifurcation. In the present problem the velocity ratio of the jet shear layer serves this purpose.

Several 'easy' experiments were performed in the counterflowing jet facility to establish whether our observations might be the result of an unstable global mode. These experiments included: (i) an examination of spectral records to determine the presence of limit-cycle behaviour; (ii) obtaining the relationship between low-level external forcing and jet response to identify whether the system was self-excited; and (iii) determining whether the saturation amplitude versus velocity ratio was consistent with the dictates of the Landau equation, indicating a supercritical Hopf bifurcation. These three experiments will be examined below for the present problem. Huerre & Monkewitz (1990) pointed out that uncontrolled external forcing, such as high background turbulence levels, can obscure the identification of global instabilities by these methods. Despite the low residual turbulence level in our facility at the jet exit plane, the disturbance level in the shear layer increases with downstream distance because the mixing layer is an effective spatial amplifier. Consequently, the observations described below are relatively 'clean' so long as the flow is examined within the first two disturbance wavelengths.

The findings of the first experiment described above were reported in §5.2, where velocity spectral data were studied in the neighbourhood of R_{cr}. One of the most striking features of the transition at $R_{cr} = 1.32$ is the formation of discrete peaks in the power spectrum (see figures 8, 9, 10). The peak power level of the velocity fluctuations at $R = 1.4$ rises more than three orders of magnitude above the surrounding background, in distinct contrast to the spectrum at $R = 1.2$ which shows a disturbance distributed over a band of frequencies (i.e. no overwhelmingly dominant peaks). The strength of the fundamental (figure 13) and the corresponding suppression of the subharmonic (figure 14) indicate that the oscillations we observe are the footprints of organized vortical structures in the jet shear layers and are reminiscent of observations made in shear layers with monochromatic forcing. However, the appearance of discrete spectral peaks, obtained by single-point hot-wire measurements, does not provide sufficient evidence to conclude that global oscillations have emerged. One must rule out the possibility that the oscillations are the consequence of a very narrowband spatial instability.

A second experiment was therefore used to determine the influence of external forcing on the strength of oscillations in the jet shear layers and, thereby, establish whether the jet response is due to self-excitation or the continuous spatial amplification of disturbances from upstream. If the jet is dominated by only

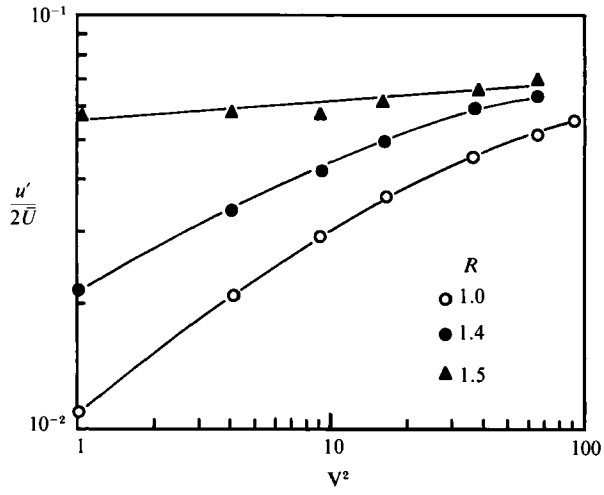

FIGURE 22. Response of the mixing layer to monochromatic forcing. Forcing was applied by a single speaker positioned at $x/D = 10$ and approximately 10 diameters off-axis of the jet. The forcing frequency was selected from the naturally occurring instability mode from figure 10(*b*).

spatially amplifying disturbances for $R < R_{cr}$ (all global modes damped), we expect that the shear layer response to external excitation will be proportional to the forcing amplitude, as Freymuth (1966) and Morkovin & Paranjape (1971) demonstrated by acoustically forcing a circular jet ($R = 1$). If a global mode emerges for $R > R_{cr}$, the flow would become overwhelmed by a time-amplifying perturbation, which would eventually saturate and render the flow insensitive to low-level external forcing. This remark must be qualified to some extent when interpreting the flow response in the immediate positive neighbourhood of R_{cr}. Owing to the small saturation amplitudes reached for slightly supercritical flows, even low-level forcing may have a significant effect on the observed disturbance level.

Jet excitation is provided by a single speaker mounted approximately 10 diameters downstream and off-axis of the jet, and the flow response is monitored by a hot wire positioned in the high-speed side of the shear layer at $x/D = 0.2$. The forcing frequency is tuned to match the naturally most amplified oscillation observed in the shear layer without forcing, as described earlier in figure 10(*b*). The shear-layer response is plotted against the r.m.s. input power to the speaker in figure 22 for velocity ratios of 1, 1.4, and 1.5. For a mixing layer without suction ($R = 1$) the shear-layer response is proportional to the speaker power, a dependence which is approximately linear for small levels of excitation. (We have assumed that the sound pressure level at the nozzle lip – where the coupling between vortical and acoustic waves is most efficient – is proportional to the input power to the speaker, although this dependence was not quantified.) In contrast to the 'linear-amplifier' behaviour displayed at $R = 1$, the mixing layer is quite insensitive to the excitation level at $R = 1.5$. Reiterating the above discussion, we believe that this insensitivity is caused by the temporal amplification and saturation of a global mode. Similar behaviour was observed in bluff-body wakes and low-density jets (Sreenivasan *et al.* 1987, 1989; Monkewitz *et al.* 1990) under supercritical conditions. Although earlier predictions place the critical velocity ratio near 1.32, there remains a rather strong dependence of the shear-layer response on the excitation level at $R = 1.4$, presumably because the state is only slightly supercritical. We note that the saturation amplitudes

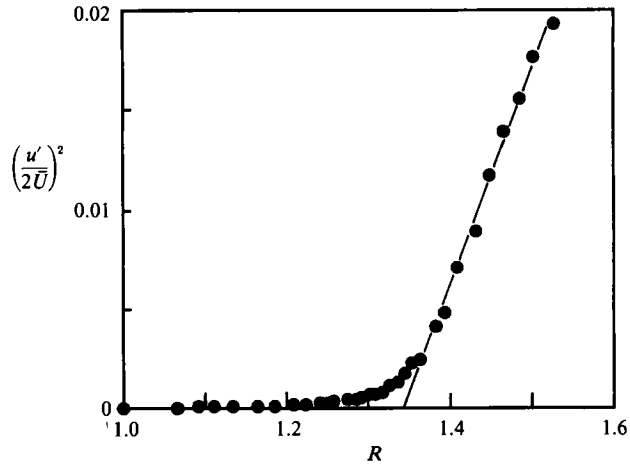

FIGURE 23. The saturation amplitude measured at the fixed spatial position of $x/D = 0.26$ on the high-speed side of the mixing layer; $U_1 = 2000$ cm/s. The linear relationship between $(u'/2\bar{U})^2$ and R can be extrapolated to locate $R_{cr} = 1.34$ at $u' = 0$.

reached at $R = 1.4$ are not significantly larger than those measured at $R = 1.3$; recall figure 13.

Finally, a third experiment was performed to establish whether the bifurcation occurring at R_{cr} might be of the supercritical Hopf type and, in particular, if the features accompanying the instability could be modelled by the Landau equation. To unambiguously identify the nature of the bifurcation, it is necessary to compute the complex constants of the Landau equation and show their invariance with spatial position in the flow. This complete analysis requires a transient investigation of the disturbance amplitude from its onset through saturation, although several features of the bifurcation can already be identified by monitoring the variation of saturation amplitude with the jet velocity ratio (control parameter). Here we will provide a brief introduction to those aspects of the Landau equation relevant to the saturation amplitude of the flow oscillations and refer the reader to Stuart (1958), Drazin & Reid (1981), and Huerre & Monkewitz (1990) for more detailed discussions.

The forced Landau equation for the disturbance amplitude $|A|$ of the global oscillations can be written in the form

$$\frac{\mathrm{d}|A|}{\mathrm{d}t} = a_1|A| - a_2|A|^3 + \alpha. \tag{7.1}$$

The constant a_1 determines the temporal amplification rate during the period of exponential growth when the bifurcation is supercritical, namely when $a_2 > 0$ and $R > R_{cr}$. When there is no forcing of the system (i.e. when $\alpha = 0$), the saturation amplitude $|A|_0$ depends on the velocity ratio in the fashion

$$|A|_0(\alpha = 0) \approx a_3(R - R_{cr})^{\frac{1}{2}}; \quad R \geqslant R_{cr}, \tag{7.2}$$

where a_3 is a positive constant which can be expressed in terms of a_1 and a_2. To determine whether (7.2) is appropriate in the present problem a hot wire was positioned in the shear layer of the jet and recorded the r.m.s. saturation amplitude of the velocity fluctuations as a function of velocity ratio. The data have been plotted in figure 23 and reveal that (7.2) describes the supercritical saturation amplitude quite well. Anticipating that background noise will influence the amplitude in the

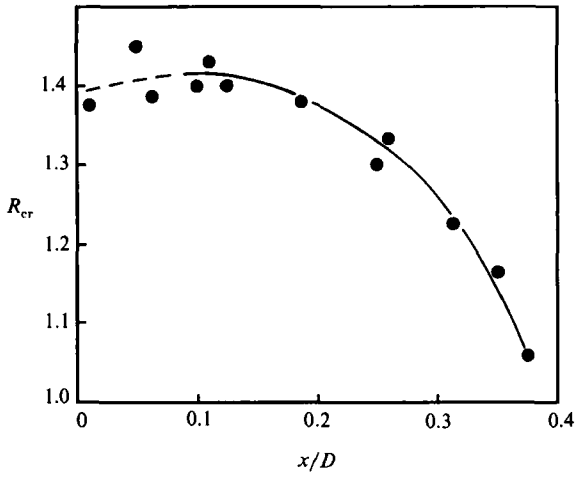

FIGURE 24. The critical velocity ratio predicted by an extrapolation of the data $(u'/2\bar{U})^2$ versus R.

immediate positive neighbourhood of R_{cr}, we can extrapolate the linear amplitude dependence in figure 23 to predict the critical velocity ratio when $|A|_0 = 0$ (the saturation amplitude $|A|_0$ equals $u'/2\bar{U}$ in the present problem).

If the Landau equation can describe the supercritical behaviour of the oscillations, then the saturation amplitude must be proportional to $(R-R_{cr})^{\frac{1}{2}}$ everywhere in the flow, and an extrapolation of the data must yield consistent estimates of R_{cr}. To verify this behaviour we measured the disturbance amplitude at various streamwise positions in the shear layer and plotted them as in figure 23. In general, we observed that the saturation amplitude was proportional to $(R-R_{cr})^{\frac{1}{2}}$ sufficiently far from the critical point, although the predicted critical velocity ratio varied in the streamwise direction, as shown in figure 24. To explain these trends it is necessary to reconsider the forced Landau equation given by (7.1).

For sufficiently low levels of forcing $[\alpha \ll |A|_0^3(\alpha = 0)]$, the saturation amplitude can be written as

$$|A|_0(\alpha) \approx a_3(R-R_{cr})^{\frac{1}{2}} + \frac{\alpha}{2a_3^2(R-R_{cr})}; \quad R > R_{cr}. \tag{7.3}$$

A close examination of (7.3) reveals that a non-zero forcing amplitude will always result in an underprediction of R_{cr} from a plot of $|A|_0^2$ versus $(R-R_{cr})$. In addition, the predicted magnitude of R_{cr} will decrease as α increases. In laboratory flows the forcing term is supplied by uncontrolled background disturbances, the amplitude of which at any given location in the flow is determined by the total amplification experienced up to that point. As an example, the total spatial amplification in the jet shear layers at subcritical velocity ratios can be quite substantial, resulting for instance in a fundamental amplitude of approximately 5% at $x/D = 0.4$ in a jet having $R = 1.2$. Therefore, since the total spatial amplification in the jet shear layers increases in the streamwise direction, we anticipate that the local forcing will increase also, resulting in larger underpredictions of R_{cr}; this is the trend observed in figure 24. As we approach the nozzle exit, the local forcing does not obscure the emergence of the global mode and provides estimates of the critical velocity ratio in the neighbourhood of 1.4. It is unclear why the prediction of R_{cr} from figure 24 differs from our earlier estimates of $R_{cr} = 1.32$ from figures 10 and 18. There is a sizeable

scatter in the data very close to the nozzle because the amplitudes are much lower there and to some extent because of probe interference, but we have not yet attempted to quantify these effects. We are possibly applying (7.3) too far from the critical point. For instance, if we were to extrapolate the curve in figure 23 using only the data between $1.3 \leqslant R \leqslant 1.35$, we would obtain a value of R_{cr} closer to 1.3. In any event, we can conclude two important observations from figures 23 and 24. First, the saturation amplitude is proportional to $(R-R_{cr})^{\frac{1}{2}}$, which is strong circumstantial evidence that the bifurcation is of the supercritical Hopf type; and second, the general behaviour seen in figure 24 is consistent with the dictates of the forced Landau equation. Clearly, the total spatial amplification of background disturbances in the jet is substantial and will vary from one jet to another depending on initial conditions. In the future, it will be necessary to quantify these effects in more detail if we expect to apply a theoretical model to a laboratory flow.

The evidence provided above does not furnish conclusive proof that the bifurcation observed at R_{cr} is the consequence of an unstable global mode; this can only be achieved by including an investigation of the transient flow response. We believe, however, that the evidence strongly suggests the existence of a supercritical Hopf bifurcation at R_{cr}. Transient experiments are currently underway in our laboratory to positively identify the bifurcation.

8. Concluding remarks

Some of the features of a spatially developing countercurrent mixing layer in a circular jet have been examined. The motivation for this work came in part from the general lack of available data on countercurrent mixing layers but principally because of the expectation that an unstable global mode would emerge at elevated velocity ratios, when the mixing layer became locally absolutely unstable (Huerre & Monkewitz 1985). We documented the onset of energetic oscillations in the jet shear layers at a critical velocity ratio of $R_{cr} = 1.32$, the power spectrum of which was essentially discrete in nature. The strength of the fundamental wave and subsequent suppression of the subharmonic suggested that these self-excited oscillations were the consequence of organized vortices in the mixing layer. Premature saturation and subsequent breakdown of the vortical structures near the nozzle prevented larger saturation amplitudes from being achieved farther downstream, thereby inhibiting the entrainment of irrotational fluid and reducing the spread rate of the mixing layer. A very similar description was given by Zaman & Hussain (1981) for the behaviour they observed in an axisymmetric mixing layer under conditions of forced excitation.

Careful consideration was given to the notion of whether the oscillations observed at supercritical velocity ratios were the result of an unstable global mode in the jet. The discrete frequency response of the mixing layer was reminiscent of the limit-cycle behaviour documented in other open-flow systems including bluff-body wakes and heated jets, but it was necessary to rule out the possibility that the oscillations were the result of a very narrowband spatial instability. To determine the self-excited nature of the bifurcation at R_{cr} we applied monochromatic forcing to the jet and observed that the mixing layer was an effective spatial amplifier for $R < R_{cr}$. This observation corroborated previous observations made in mixing layers at a unity velocity ratio (Freymuth 1966; Morkovin & Paranjape 1971). With the exception of slightly supercritical velocity ratios, the flow response for $R > R_{cr}$ was essentially insensitive to external forcing, indicating the self-excited nature of the system. Finally, we attempted to model the bifurcation with the purely temporal

Landau equation by establishing some features of the saturation state of the oscillations. We found that the saturation amplitude was proportional to $(R-R_{cr})^{\frac{1}{2}}$ throughout the flow domain, indicating the presence of a supercritical Hopf bifurcation. However, predictions of R_{cr} from the data were inconsistent, displaying a strong dependence on streamwise position. We believe that the spatial amplification of background disturbances provided local forcing of the layer, the magnitude of which increased in the streamwise direction. The Landau equation revealed that this forcing would result in underpredictions of the critical velocity ratio, a trend supported by our data. If this argument is correct, the data very close to the nozzle exit should provide the cleanest estimate of R_{cr}, but the value of $R_{cr} \approx 1.4$ (figure 24) obtained in this fashion is inconsistent with all other estimates of the transition occurring at $R_{cr} = 1.32$. We have not ruled out probe interference as a principal cause of the discrepancy, but until such effects can be quantified, other physical explanations should not be disregarded, including the possible inadequacies of applying the Landau model to the present problem.

The agreement between the experimentally determined bifurcation point of $R_{cr} = 1.32$ and the convective/absolute transition predicted from local linear stability theory of $R_{cr} = 1.315$ is encouraging. But, we must emphasize that this result is to some extent fortuitous, given our *ad hoc* definition of R. At $R_{cr} = 1.32$ the local velocity ratio varies between 1.36 and 1.27 in the first two disturbance wavelengths where exponential growth is observed (i.e. where the linear theory is valid). This indicates that a finite region of locally absolutely unstable flow must exist in the jet before the onset of global instability, as Chomaz *et al.* (1988) predicted. When this region of absolutely unstable flow is reduced, the flow will become marginally globally unstable before becoming convectively unstable everywhere. The amplification of the pure spectral peak at slightly subcritical velocity ratios (e.g. at $R = 1.3$ in figure 9) could be the consequence of background forcing on the marginally globally unstable jet.

Measurement uncertainty will also influence our results. We believe that the largest uncertainty was associated with the data gathered in the reverse flow stream as a consequence of the hot-wire probe orientation. We have tried to minimize these effects whenever possible, but more detailed measurements, preferably with a non-intrusive probe, are clearly needed. The scaling parameters of θ_0, $\bar{U}$, and ΔU depend on the magnitude of the reverse flow stream, and the shape of the velocity profile, and their numerical values will affect our estimates of $R_{cr} = 1.32$. The important conclusion of this study, however, is that the transition we observed is quite robust and independent of precisely how we define these parameters. The bifurcation point and the supercritical saturation state of the flow, on the other hand, will depend on the details of the two-dimensional velocity field as a result of changes in the initial and boundary conditions of the forward and suction streams (e.g. changes in slot width and nozzle design). Streamwise variations in the velocity ratio and momentum thickness will influence the wave dispersion characteristics in the near field of the jet (and therefore vortex pairing), and must be examined separately for each flow under investigation. As an example, if suction were applied to the shear layers of a jet with very thick shear layers (e.g. a nearly parabolic jet), the strong coupling between the jet shear layer and column modes might result in a completely different saturation state for supercritical velocity ratios than we documented here. (We are assuming that a global instability can be established in such a jet with counterflow, but there is currently no evidence to indicate that this is the case.)

The flow response at R_{cr} was described as 'self-excited'. The justification for this

description came in part from the spatial growth-rate data in figure 13. At supercritical velocity ratios, the data were not uniquely characterized by the spatial scale Rx/λ, but displayed elevated amplitudes reminiscent of the forcing experiments of Freymuth (1966). The following heuristic model captures the essential features of the spatio-temporal behaviour at R_{cr}. When the flow is globally stable ($R < R_{cr}$), there is a continuous spatial amplification of the background disturbances as they enter the flow domain from upstream; this spatial growth was observed in figure 11. At the onset of global instability ($R = R_{cr}$), a stationary disturbance source is switched 'on' in the flow field (this source represents the global mode). The output amplitude from this source grows temporally, until a saturation level is reached, after which time the forcing amplitude remains constant. (The magnitude of excitation increases with $R-R_{cr}$ as shown in figure 13; the dependence is given in figure 23.) The fluid disturbances created by the stationary source experience spatial amplification in the same way as the background disturbances. This is why we observe well-defined spatial growth at $R > R_{cr}$ in figure 13. If the amplitude from the source were extremely large, the region of exponential growth could be bypassed completely. Furthermore, the spectral behaviour we observe at $R > R_{cr}$ is characteristic of the disturbances originating at the stationary source. If the source could be switched 'off', we would again observe the continuous spatial amplification of the background disturbances, which are otherwise masked.

At present there are no reliable methods of predicting what the saturation state of a flow will be after global instability has set in. Therefore, if the flow response must be examined on a case-to-case basis, what have we learned about counterflowing jets that can be used to manipulate a more general class of spatially developing free-shear flows? The most important result of this study is that the jet could be controlled/modified dramatically by relying entirely on our expectations from the linear stability theory. We were able to produce self-excited oscillations by establishing conditions of local absolute instability in a finite region of the jet. Consequently, the vortical motion in the laminar shear layer became quite organized without relying on external monochromatic forcing. This approach has the advantage of not requiring knowledge of the forcing frequency and thereby eliminating complicated feedback control schemes. Finally, we believe this approach may prove to be successful in 'organizing' the structures in turbulent separated layers where forcing levels attainable by acoustic or mechanical means are typically too low to be effective.

The authors would like to thank Mr David Ouyang for his careful assistance with the data acquisition. The work was supported through the Grants-in-Aid program of the Graduate School of the University of Minnesota.

REFERENCES

BECHERT, D. W. 1985 Excitation of instability waves. *Z. Flugwiss. Weltraumforsch.* **9**, 356–361.

BECKER, H. A. & MASSARO, T. A. 1968 Vortex evolution in a round jet. *J. Fluid Mech.* **31**, 435–448.

BRADSHAW, P. 1966 The effect of initial conditions on the development of a free shear layer. *J. Fluid Mech.* **26**, 225–236.

BROWN, G. L. & ROSHKO, A. 1974 On density effects and large structure in turbulent mixing layers. *J. Fluid Mech.* **64**, 775–816.

CHOMAZ, J. M., HUERRE, P. & REDEKOPP, L. G. 1988 Bifurcations to local and global modes in spatially-developing flows. *Phys. Rev. Lett.* **60**, 25–28.

CORKE, T., KOGA, D., DRUBKA, R. & NAGIB, H. 1977 A new technique for introducing controlled sheets of smoke streaklines in wind tunnels. *Proc. ICIASF, IEEE 77CH1251-8 AES*, pp. 74–80.

CROW, S. C. & CHAMPAGNE, F. H. 1971 Orderly structure in jet turbulence. *J. Fluid Mech.* **48**, 547–591.

DRAZIN, P. G. & REID, W. H. 1981 *Hydrodynamic stability*. Cambridge University Press.

DRUBKA, R. E. & NAGIB, H. M. 1981 Instabilities in near field of turbulent jets and their dependence on initial conditions and Reynolds number. *Tech. Rep.* AFOSR-TR-82. Illinois Institute of Technology, Chicago.

DRUBKA, R. E., REISENTHEL, P. & NAGIB, H. M. 1989 The dynamics of low initial disturbance turbulent jets. *Phys. Fluids* A **1**, 1723–1735.

FREYMUTH, P. 1966 On the transition in a separated laminar boundary layer. *J. Fluid Mech.* **25**, 683–704.

HANNEMANN, K. & OERTEL, H. 1989 Numerical simulation of the absolutely and convectively unstable wake. *J. Fluid Mech.* **199**, 55–88.

HO, C.-M. & HUANG, L.-S. 1982 Subharmonics and vortex merging in mixing layers. *J. Fluid Mech.* **119**, 443–473.

HO, C.-M. & HUERRE, P. 1984 Perturbed free shear layers. *Ann. Rev. Fluid Mech.* **16**, 365–424.

HUERRE, P. & MONKEWITZ, P. A. 1985 Absolute and convective instabilities in free shear layers. *J. Fluid Mech.* **159**, 151–168.

HUERRE, P. & MONKEWITZ, P. A. 1990 Local and global instabilities in spatially developing flows. *Ann. Rev. Fluid Mech.* **22**, 473–537.

HUMPHREY, J. A. C. & LI, S. 1981 Tilting, stretching, pairing and collapse of vortex structures in confined counter-current flows. *Trans. ASME* I: *J. Fluids Engng* **101**, 466–470.

HUSAIN, Z. D. & HUSSAIN, A. K. M. F. 1979 Axisymmetric mixing layer: influence of the initial and boundary conditions. *AIAA J.* **17**, 48–55.

HUSSAIN, A. K. M. F. & ZAMAN, K. B. M. Q. 1978 The free shear layer tone phenomenon and probe interference. *J. Fluid Mech.* **87**, 349–383.

JACKSON, C. P. 1987 A finite-element study of the onset of vortex shedding in flow past variously shaped bodies. *J. Fluid Mech.* **182**, 23–45.

KARNIADAKIS, G. E. & TRIANTAFYLLOU, G. S. 1989 Frequency selection and asymptotic states in laminar wakes. *J. Fluid Mech.* **199**, 441–469.

KELLY, R. E. 1967 On the stability of an inviscid shear layer which is periodic in space and time. *J. Fluid Mech.* **27**, 657–689.

KIBENS, V. 1989 Jet flows and turbulence control. *McDonnell Douglas Research Laboratories Rep.* MDRL 89-106.

KOCH, W. 1985 Local instability characteristics and frequency determination of self-excited wake flows. *J. Sound Vib.* **99**, 53–83.

KYLE, D. & SREENIVASAN, K. R. 1989 Stability properties of He/air jets. *Proc. ASME Fluids Engng Spring. Conf., La Jolla.*

MATHIS, C., PROVANSAL, M. & BOYER, L. 1984 The Bénard-von Kármán instability: an experimental study near the threshold. *J. Phys. Lett.* **45**, 483–491.

MICHALKE, A. 1964 On the inviscid instability of the hyperbolic tangent velocity profile. *J. Fluid Mech.* **19**, 543–556.

MICHALKE, A. 1965 On spatially growing disturbances in an inviscid shear layer. *J. Fluid Mech.* **23**, 521–544.

MICHALKE, A. 1971 Instabilität eines kompressiblen runden Freistrahls under Berücksichtigung des Einflusses der Strahlgrenzschichtdicke. *Z. Flugwiss.* **19**, 319–328.

MIKSAD, R. W. 1972 Experiments on the nonlinear stages of free shear layer transition. *J. Fluid Mech.* **56**, 695–719.

MONKEWITZ, P. A. 1988 The absolute and convective nature of instability in two-dimensional wakes at low Reynolds numbers. *Phys. Fluids* **31**, 999–1006.

MONKEWITZ, P. A., BECHERT, D. W., BARSIKOW, B. & LEHMANN, B. 1990 Self-excited oscillations and mixing in a heated round jet. *J. Fluid Mech.* **213**, 611–639.

MONKEWITZ, P. A. & HUERRE, P. 1982 The influence of the velocity ratio on the spatial instability of mixing layers. *Phys. Fluids* **25**, 1137–1143.

MONKEWITZ, P. A. & NGUYEN, L. N. 1987 Absolute instability in the near wake of two-dimensional bluff bodies. *J. Fluids Struct.* **1**, 165–184.

MONKEWITZ, P. A. & SOHN, K. D. 1988 Absolute instability in hot jets. *AIAA J.* **26**, 911–916.

MORKOVIN, M. & PARANJAPE, S. V. 1971 Acoustic excitation of shear layers. *Z. Flugwiss.* **19**, 328–335.

NICCUM, D. L. 1990 The influence of velocity ratio on a counterflowing circular jet. M.S. thesis, University of Minnesota.

PERRY, A. E. & LIM, T. T. 1978 Coherent structures in coflowing jets and wakes. *J. Fluid Mech.* **88**, 451–463.

PERRY, A. E., LIM, T. T. & CHONG, M. S. 1980 The instantaneous velocity fields of coherent structures in coflowing jets and wakes. *J. Fluid Mech.* **101**, 243–256.

PETERSEN, R. A. 1978 Influence of wave dispersion on vortex pairing in a jet. *J. Fluid Mech.* **89**, 469–495.

PROVANSAL, M., MATHIS, C. & BOYER, L. 1987 Bénard–von Kármán instability: transient and forced regimes. *J. Fluid Mech.* **182**, 1–22.

RAMAN, G., ZAMAN, K. B. M. Q. & RICE, E. J. 1989 Initial turbulence effect on jet evolution with and without tonal excitation. *Phys. Fluids* A **1**, 1240–1248.

RAMSHANKAR, R. 1988 The dynamics of countercurrent mixing layers. Ph.D. thesis, Yale University.

SREENIVASAN, K. R., RAGHU, S. & KYLE, D. 1989 Absolute instability in variable density round jets. *Exp. Fluids* **7**, 309–317.

SREENIVASAN, K. R., STRYKOWSKI, P. J. & OLINGER, D. J. 1987 Hopf bifurcation, Landau equation and vortex shedding behind circular cylinders. In *Proc. Forum Unsteady Flow Sep.* (ed. K. Ghia), vol. 52, pp. 1–13. ASME.

STRYKOWSKI, P. J. & NICCUM, D. L. 1989 Turbulence suppression in axisymmetric counterflowing jets by self-excitation. *Bull. Am. Phys. Soc.* **34**, 2326 (abstract only).

STRYKOWSKI, P. J. & SREENIVASAN, K. R. 1990 On the formation and suppression of vortex 'shedding' at low Reynolds numbers. *J. Fluid Mech.* **218**, 71–107.

STUART, J. T. 1958 On the nonlinear mechanics of hydrodynamic stability. *J. Fluid Mech.* **4**, 1–21.

TAN-ATICHAT, J. 1980 Effects of axisymmetric contractions of various scales. Ph.D. thesis, Illinois Institute of Technology.

THORPE, A. S. 1968 A method of producing a shear flow in a stratified fluid. *J. Fluid Mech.* **32**, 693–704.

THORPE, A. S. 1971 Experiments on instability and turbulence in a stratified shear flow: miscible fluids. *J. Fluid Mech.* **46**, 299–319.

WILLE, R. 1963 Beiträge zur Phänomenologie der Freistrahlen. *Z. Flugwiss.* **11**, 222–233.

WINANT, C. D. & BROWAND, F. K. 1974 Vortex pairing, the mechanism of turbulent mixing-layer growth at moderate Reynolds number. *J. Fluid Mech.* **63**, 237–255.

ZAMAN, K. B. M. Q. & HUSSAIN, A. K. M. F. 1980 Vortex pairing in a circular jet under controlled excitation. Part 1. General jet response. *J. Fluid Mech.* **101**, 449–491.

ZAMAN, K. B. M. Q. & HUSSAIN, A. K. M. F. 1981 Turbulence suppression in free shear flows by controlled excitation. *J. Fluid Mech.* **103**, 133–159.

ZEBIB, A. 1987 Stability of viscous flow past a circular cylinder. *J. Engng Maths* **21**, 155–165.